1 Theory

1.1 Three-band tight-binding model

In the model introduced by Liu *et al.*, only the orbitals of the M atom are included. We denote the wave functions of the three orbitals of the M atom as

$$|\phi_1\rangle = |d_{z^2}\rangle\,, \quad |\phi_2\rangle = \left|d_{xy}\right\rangle, \quad |\phi_3\rangle = \left|d_{x^2-y^2}\right\rangle. \tag{1}$$

The Bloch wavefunction in this model has the form

$$\psi^{\lambda}_{\mathbf{k}}(\mathbf{r}) = \sum_{j=1}^{3} C^{\lambda}_{j}(\mathbf{k}) \sum_{\mathbf{R}} e^{i\mathbf{k}\cdot\mathbf{R}} \phi_j(\mathbf{r}-\mathbf{R}). \tag{2}$$

The coefficents $C^{\lambda}_{j}(\mathbf{k})$ are the solutions of the eigenvalue equation

$$\sum_{jj'}^{3} \left[H^{\mathrm{TB}}_{jj'}(\mathbf{k}) - \varepsilon_{\lambda}(\mathbf{k}) S_{jj'}(\mathbf{k}) \right] C^{\lambda}_{j}(\mathbf{k}) = 0, \tag{3}$$

where

$$H^{\mathrm{TB}}_{jj'}(\mathbf{k}) = \sum_{\mathbf{R}} e^{i\mathbf{k}\cdot\mathbf{R}} \left\langle \phi_j(\mathbf{r}) \right| H_{1\mathrm{e}} \left| \phi_{j'}(\mathbf{r}-\mathbf{R}) \right\rangle, \tag{4}$$

and

$$S_{jj'}(\mathbf{k}) = \sum_{\mathbf{R}} \left\langle \phi_j(\mathbf{r}) \middle| \phi_{j'}(\mathbf{r}-\mathbf{R}) \right\rangle \approx \delta_{jj'}. \tag{5}$$

In the case $B \neq 0$, the wavefunction has an additional phase factor

$$\psi^{\lambda}_{\mathbf{k}}(\mathbf{r}) = \sum_{j=1}^{3} C^{\lambda}_{j} \sum_{\mathbf{R}} e^{i\mathbf{k}\cdot\mathbf{R}} e^{i\theta_{\mathbf{R}}(\mathbf{r})} \phi_j(\mathbf{r}-\mathbf{R}), \tag{6}$$

and choose $\theta = -\frac{e}{\hbar}\int_{\mathbf{r}}^{\mathbf{R}} \mathbf{A}(\mathbf{r}') \cdot d\mathbf{r}'$ as Peierls phase factor, the Hamiltonian now is

$$H_{jj'} = \sum_{\mathbf{R}} e^{i\mathbf{k}\cdot\mathbf{R}} e^{\frac{ie}{\hbar}\int_{0}^{\mathbf{R}} \mathbf{A}(\mathbf{r})\cdot d\mathbf{r}} E_{jj'}(\mathbf{R}), \tag{7}$$

where

$$E_{jj'} = \left\langle \phi_j(\mathbf{r}) \right| H_{1e} \left| \phi_{j'}(\mathbf{r}-\mathbf{R}) \right\rangle. \tag{8}$$

Using a uniform magnetic field $\mathbf{B} = (0, 0, B)$ and Landau gauge $\mathbf{A} = (By, 0, 0)$. The

Peierls hopping phase is given

$$\begin{aligned}\frac{ie}{\hbar}\int_{\mathbf{0}}^{\mathbf{R}}\mathbf{A}(\mathbf{r})\cdot d\mathbf{r} &= \frac{ie}{\hbar}\int_{\mathbf{0}}^{\mathbf{R}} Bydx \\ &= \frac{ieB}{\hbar}\int_0^1 y(\tau)x'(\tau)d\tau,\end{aligned} \tag{9}$$

suppose that the atom M is located at lattice vector $\mathbf{R}_{m,n}$, the Peierls phase can be written as

$$\theta_{m,n}^{m',n'} = \begin{cases} 0 & m' = m \pm 2, n' = n, \\ 0 & m' = m \pm 4, n' = n, \\ \pm\frac{e}{\hbar}\frac{Ba^2\sqrt{3}}{2}m & m' = m, n' = n \pm 2, \\ \pm\frac{e}{\hbar}\frac{Ba^2\sqrt{3}}{4}\left(m \mp \frac{1}{2}\right) & m' = m \mp 1, n' = n \pm 1, \\ \pm\frac{e}{\hbar}\frac{Ba^2\sqrt{3}}{2}(m \mp 1) & m' = m \mp 2, n' = n \pm 2, \\ \pm\frac{e}{\hbar}\frac{Ba^2\sqrt{3}}{4}\left(m \mp \frac{3}{2}\right) & m' = m \mp 3, n' = n \pm 1. \end{cases} \tag{10}$$

We obtain the Hamiltonian in magnetic field

$$\begin{aligned} H_{jj'}^{\mathrm{TB}}(\mathbf{k}) = {} & E_{jj'}(\mathbf{0}) + e^{i\mathbf{k}\cdot\mathbf{R}_1}E_{jj'}(\mathbf{R}_1) + e^{-i\pi(m+1/2)\frac{\Phi}{\Phi_0}}e^{i\mathbf{k}\cdot\mathbf{R}_2}E_{jj'}(\mathbf{R}_2) \\ & + e^{-i\pi(m-1/2)\frac{\Phi}{\Phi_0}}e^{i\mathbf{k}\cdot\mathbf{R}_3}E_{jj'}(\mathbf{R}_3) + e^{i\mathbf{k}\cdot\mathbf{R}_4}E_{jj'}(\mathbf{R}_4) \\ & + e^{i\pi(m-1/2)\frac{\Phi}{\Phi_0}}e^{i\mathbf{k}\cdot\mathbf{R}_5}E_{jj'}(\mathbf{R}_5) + e^{i\pi(m+1/2)\frac{\Phi}{\Phi_0}}e^{i\mathbf{k}\cdot\mathbf{R}_6}E_{jj'}(\mathbf{R}_6) \\ & + e^{-i\pi(m+3/2)\frac{\Phi}{\Phi_0}}e^{i\mathbf{k}\cdot\mathbf{R}_7}E_{jj'}(\mathbf{R}_7) + e^{-2i\pi m\frac{\Phi}{\Phi_0}}e^{i\mathbf{k}\cdot\mathbf{R}_8}E_{jj'}(\mathbf{R}_8) \\ & + e^{-i\pi(m-3/2)\frac{\Phi}{\Phi_0}}e^{i\mathbf{k}\cdot\mathbf{R}_9}E_{jj'}(\mathbf{R}_9) + e^{i\pi(m-3/2)\frac{\Phi}{\Phi_0}}e^{i\mathbf{k}\cdot\mathbf{R}_{10}}E_{jj'}(\mathbf{R}_{10}) \\ & + e^{2i\pi m\frac{\Phi}{\Phi_0}}e^{i\mathbf{k}\cdot\mathbf{R}_{11}}E_{jj'}(\mathbf{R}_{11}) + e^{i\pi(m+3/2)\frac{\Phi}{\Phi_0}}e^{i\mathbf{k}\cdot\mathbf{R}_{12}}E_{jj'}(\mathbf{R}_{12}) \\ & + e^{i\mathbf{k}\cdot\mathbf{R}_{13}}E_{jj'}(\mathbf{R}_{13}) + e^{-2i\pi(m+1)\frac{\Phi}{\Phi_0}}e^{i\mathbf{k}\cdot\mathbf{R}_{14}}E_{jj'}(\mathbf{R}_{14}) \\ & + e^{-2i\pi(m-1)\frac{\Phi}{\Phi_0}}e^{i\mathbf{k}\cdot\mathbf{R}_{15}}E_{jj'}(\mathbf{R}_{15}) + e^{i\mathbf{k}\cdot\mathbf{R}_{16}}E_{jj'}(\mathbf{R}_{16}) \\ & + e^{2i\pi(m-1)\frac{\Phi}{\Phi_0}}e^{i\mathbf{k}\cdot\mathbf{R}_{17}}E_{jj'}(\mathbf{R}_{17}) + e^{2i\pi(m+1)\frac{\Phi}{\Phi_0}}e^{i\mathbf{k}\cdot\mathbf{R}_{18}}E_{jj'}(\mathbf{R}_{18}), \end{aligned} \tag{11}$$

where $\Phi_0 = \frac{h}{e}$ and $\Phi = \frac{\sqrt{3}}{2}Ba^2$. Since the Peierls phase depends on the the atomic position specified by the site indices m, n, the Hamiltonian is no longer invariant under translation of a primitive vector. For the case $\frac{\Phi}{\Phi_0} = \frac{p}{q}$, with $p, q \in \mathbb{Z}$, it is possible to restore the translational invariance if we expand the unit cell so that it includes $2q$ M atoms. We, then, define a new basis set of $6q$ atomic orbitals $\left\{\phi_j(\mathbf{r} - \mathbf{R}_{m,n})\right\}$. The wave

function can be expressed as the coefficients of C_{ji}^{λ} in the tight-binding wave function

$$\psi_{\mathbf{k}}^{\lambda}(\mathbf{r}) = \sum_{j}^{3} \sum_{i}^{2q} C_{ji}^{\lambda}(\mathbf{k}) \sum_{\mathbf{R}} e^{\frac{ie}{\hbar}\int_{0}^{\mathbf{R}+\mathbf{R}_i} \mathbf{A}(\mathbf{r})\cdot d\mathbf{r}} e^{i\mathbf{k}\cdot(\mathbf{R}+\mathbf{R}_i)} \phi_j(\mathbf{r}-\mathbf{R}-\mathbf{R}_i). \tag{12}$$

where $j = 1, 2, 3$ and i labels the atom $\mathbf{R}_i$ in the magnetic unit cell, with $i = 1, \ldots, 2q$, and the new lattice vector now is $\mathbf{R} = k\mathbf{a}_1 + l2q\mathbf{a}_2$, where $k, l \in \mathbb{Z}$. In this basis, the TB Hamiltonian has an additional Peierls phase

$$H_{jij'i'} = \sum_{\mathbf{R}} e^{i\mathbf{k}\cdot(\mathbf{R}-\mathbf{R}_i+\mathbf{R}_{i'})} e^{\frac{ie}{\hbar}\int_{\mathbf{R}_i}^{\mathbf{R}+\mathbf{R}_{i'}} \mathbf{A}(\mathbf{r})\cdot d\mathbf{r}} \left\langle \phi_j(\mathbf{r}-\mathbf{R}_i) \right| H_{1e} \left| \phi_{j'}(\mathbf{r}-\mathbf{R}-\mathbf{R}_{i'}) \right\rangle, \tag{13}$$

The sum over $\mathbf{R}$ include up to third-nearest-neighbor hoppings. It is remarkbly to note that the lattice vectors satisfying the condition $|\mathbf{R}| \leq 2a$ are $\mathbf{R} = \mathbf{0}, \pm\mathbf{a}_1, \pm 2\mathbf{a}_1$, we obtain the Hamiltonian

$$\begin{aligned}
H_{jnj'n'}^{\text{eff}}(\mathbf{k}) &= E_{jj'}(\mathbf{0})\delta_{n,n'} + e^{i\mathbf{k}\cdot\mathbf{R}_1} E_{jj'}(\mathbf{R}_1)\delta_{n,n'} + e^{i\mathbf{k}\cdot\mathbf{R}_4} E_{jj'}(\mathbf{R}_4)\delta_{n,n'} \\
&+ e^{-i\pi(m+1/2)\frac{\Phi}{\Phi_0}} e^{i\mathbf{k}\cdot\mathbf{R}_2} E_{jj'}(\mathbf{R}_2)\delta_{n-1,n'} + e^{-i\pi(m-1/2)\frac{\Phi}{\Phi_0}} e^{i\mathbf{k}\cdot\mathbf{R}_3} E_{jj'}(\mathbf{R}_3)\delta_{n-1,n'} \\
&+ e^{i\pi(m-1/2)\frac{\Phi}{\Phi_0}} e^{i\mathbf{k}\cdot\mathbf{R}_5} E_{jj'}(\mathbf{R}_5)\delta_{n+1,n'} + e^{i\pi(m+1/2)\frac{\Phi}{\Phi_0}} e^{i\mathbf{k}\cdot\mathbf{R}_6} E_{jj'}(\mathbf{R}_6)\delta_{n+1,n'} \\
&+ e^{-i\pi(m+3/2)\frac{\Phi}{\Phi_0}} e^{i\mathbf{k}\cdot\mathbf{R}_7} E_{jj'}(\mathbf{R}_7)\delta_{n-1,n'} + e^{-2i\pi m\frac{\Phi}{\Phi_0}} e^{i\mathbf{k}\cdot\mathbf{R}_8} E_{jj'}(\mathbf{R}_8)\delta_{n-2,n'} \\
&+ e^{-i\pi(m-3/2)\frac{\Phi}{\Phi_0}} e^{i\mathbf{k}\cdot\mathbf{R}_9} E_{jj'}(\mathbf{R}_9)\delta_{n-1,n'} + e^{i\pi(m-3/2)\frac{\Phi}{\Phi_0}} e^{i\mathbf{k}\cdot\mathbf{R}_{10}} E_{jj'}(\mathbf{R}_{10})\delta_{n+1,n'} \\
&+ e^{2i\pi m\frac{\Phi}{\Phi_0}} e^{i\mathbf{k}\cdot\mathbf{R}_{11}} E_{jj'}(\mathbf{R}_{11})\delta_{n+2,n'} + e^{i\pi(m+3/2)\frac{\Phi}{\Phi_0}} e^{i\mathbf{k}\cdot\mathbf{R}_{12}} E_{jj'}(\mathbf{R}_{12})\delta_{n+1,n'} \\
&+ e^{i\mathbf{k}\cdot\mathbf{R}_{13}} E_{jj'}(\mathbf{R}_{13})\delta_{n,n'} + e^{-2i\pi(m+1)\frac{\Phi}{\Phi_0}} e^{i\mathbf{k}\cdot\mathbf{R}_{14}} E_{jj'}(\mathbf{R}_{14})\delta_{n-2,n'} \\
&+ e^{-2i\pi(m-1)\frac{\Phi}{\Phi_0}} e^{i\mathbf{k}\cdot\mathbf{R}_{15}} E_{jj'}(\mathbf{R}_{15})\delta_{n-2,n'} + e^{i\mathbf{k}\cdot\mathbf{R}_{16}} E_{jj'}(\mathbf{R}_{16})\delta_{n,n'} \\
&+ e^{2i\pi(m-1)\frac{\Phi}{\Phi_0}} e^{i\mathbf{k}\cdot\mathbf{R}_{17}} E_{jj'}(\mathbf{R}_{17})\delta_{n+2,n'} + e^{2i\pi(m+1)\frac{\Phi}{\Phi_0}} e^{i\mathbf{k}\cdot\mathbf{R}_{18}} E_{jj'}(\mathbf{R}_{18})\delta_{n+2,n'}.
\end{aligned} \tag{14}$$

where $\Phi_0 = \frac{h}{e}$, $\Phi = \frac{\sqrt{3}}{2}Ba^2$ and $E(\mathbf{R})$ are obtained from Liu *et al.*

1.2 The cyclotron theory

The cyclotron frequency can be obtained from the energy difference between two Landau levels

$$\hbar\omega_c = E_{n+1} - E_n, \tag{15}$$

which gives

$$\omega_c = \frac{E_{n+1} - E_n}{\hbar}. \tag{16}$$

On the other hand, the cyclotron frequency is also defined as

$$\omega_c = \frac{eB}{m^*}. \tag{17}$$

Combining the two expressions, the effective mas can be written as

$$m^* = \frac{eB}{\omega_c} = \frac{eB}{\frac{E_{n+1}-E_n}{\hbar}} = \frac{eB\hbar}{E_{n+1}-E_n}, \tag{18}$$

and

$$\omega_c = \frac{E_{n+1}-E_n}{\hbar}. \tag{19}$$

The radius of cyclotron orbit can be written as

$$r_c = \frac{v_F}{\omega_c} = \frac{v_F\hbar}{E_{n+1}-E_n} = \frac{v_F m^*}{eB}, \tag{20}$$

where v_F is given in Table 1.

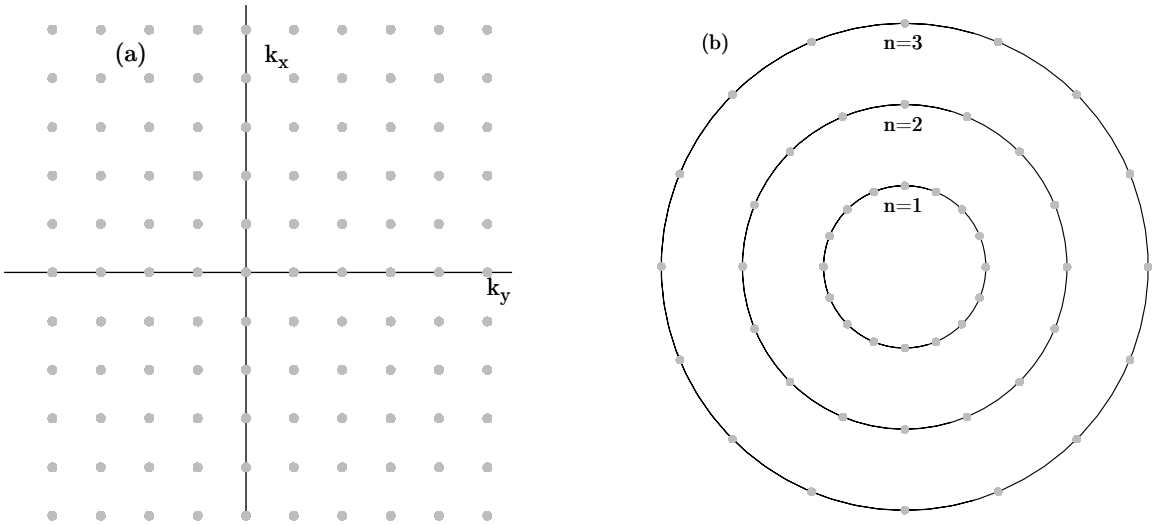

Figure 1: (a) Electron motion in two dimensions without magnetic field. (b) Under magnetic field, electrons move in circular orbits in the k-plane.

When an electron moves in a periodic crystal lattice under a magnetic field B, its motion is governed by two distinct types of periodic dynamics. The first originates from the periodic lattice potential, while the second is the cyclotron motion induced by the Lorentz force, which drives the electron into circular orbits with a cyclotron radius $r_c \propto \frac{1}{B}$. At weak magnetic fields, the cyclotron radius r_c is much larger than the lattice constant a. In this regime, the two motions—lattice periodic motion and cyclotron motion—are essentially independent, and the effective mass m^* remains nearly constant. At strong magnetic fields, however, the cyclotron radius r_c becomes comparable to the

lattice constant r_0. Consequently, the electron dynamics are strongly influenced by the interplay between the Lorentz force and the periodic lattice potential. This coupling gives rise to a variety of rich physical phenomena, such as the Hofstadter butterfly, where the Landau levels form a fractal-like structure, and modifications of the effective mass m^*. These effects may exhibit distinct behaviors in the K and K' valleys.

	$\hbar v_F$ (eVÅ)	v_F (m/s)		$\hbar v_F$ (eVÅ)	v_F (m/s)
MoS_2	2.76	4.19 $\times 10^5$	WS_2	4.38	6.65 $\times 10^5$
$MoSe_2$	2.53	3.84 $\times 10^5$	WSe_2	3.94	5.99 $\times 10^5$
$MoTe_2$	0.87	1.32 $\times 10^5$	WTe_2	2.03	3.09 $\times 10^5$

Table 1: Parameters of the effective Hamiltonian for the four common types of TMDs. The Fermi velocities are taken from Ref. [1, 2].

2 Methods

When a magnetic field is applied to the crystal lattice, the magnetic unit cell is enlarged q times for square lattice ($2q$ times for hexagonal lattice). As a consequence, the magnetic Brillouin zone smaller $2q$ times than the orginal Brillouin zone [3].

In addition, the three bases $d_{z^2}, d_{xy}, d_{x^2-y^2}$, which were introduced by Liu *et al.*, cannot clearly distinguish the K and K' points in the valence and conduction bands for two reasons. First, the squared amplitudes $|\psi|^2$ are identical. Second, in the magnetic Brillouin zone, the K and K' valleys cannot be intuitively distinguished by the dispersion relation $E(\mathbf{k})$; instead, one needs to examine the properties of the wave functions. Specifically, the electron wave function at the K valley in conduction band is mainly contributed by d_{z^2}, while at the valence band it is $d_{xy} + d_{x^2-y^2}$. Furthemore, we can distingushed K and K' valleys at the valence by using bases

$$\left|\psi_v^K\right\rangle = \frac{1}{\sqrt{2}}\left(\left|d_{x^2-y^2}\right\rangle + i\left|d_{xy}\right\rangle\right), \tag{21}$$

$$\left|\psi_v^{K'}\right\rangle = \frac{1}{\sqrt{2}}\left(\left|d_{x^2-y^2}\right\rangle - i\left|d_{xy}\right\rangle\right). \tag{22}$$

Therefore, it is necessary to adopt another basis set. We now consider a new basis consisting of the three eigenfunctions of the angular momentum operators L^2 and L_z, corresponding to $l = 2$ and $m = 0, \pm 2$.

$$\left|\tilde{\phi}_1\right\rangle = \left|d_{m=0}\right\rangle, \quad \left|\tilde{\phi}_2\right\rangle = \left|d_{m=+2}\right\rangle, \quad \left|\tilde{\phi}_3\right\rangle = \left|d_{m=-2}\right\rangle. \tag{23}$$

The new basis can be obtained from the old one by the transformation

$$\left|\tilde{\phi}_j\right\rangle = \sum_{j'} W_{j'j}\left|\phi_{j'}\right\rangle, \tag{24}$$

where

$$W = \begin{pmatrix} 1 & 0 & 0 \\ 0 & \frac{i}{\sqrt{2}} & -\frac{i}{\sqrt{2}} \\ 0 & \frac{1}{\sqrt{2}} & \frac{1}{\sqrt{2}} \end{pmatrix}. \tag{25}$$

In particular,

$$\left|\tilde{\phi}_1\right\rangle = |\phi_1\rangle\,, \tag{26}$$

$$\left|\tilde{\phi}_2\right\rangle = \frac{i}{\sqrt{2}}\,|\phi_2\rangle + \frac{1}{\sqrt{2}}\,|\phi_3\rangle\,, \tag{27}$$

$$\left|\tilde{\phi}_3\right\rangle = -\frac{i}{\sqrt{2}}\,|\phi_2\rangle + \frac{1}{\sqrt{2}}\,|\phi_3\rangle\,. \tag{28}$$

The TB Hamiltonian in new basis reads

$$\tilde{H}^{\mathrm{TB}}(\mathbf{k}) = W^{\dagger} H^{\mathrm{TB}}(\mathbf{k}) W, \tag{29}$$

where $H^{\mathrm{TB}} = H^{\mathrm{NN}}$ or H^{TNN}.

To distinguish the states that originate from the original Brillouin zone, we follow the convention of Ho *et al.* [4]. Each Landau level is then labeled as $|j, n\rangle_{\tau}$, where j, n, and τ denote the orbital, Landau, and valley indices, respectively.

Degeneracy: The degeneracy of Landau levels can be addressed by two reasons, first arises from the motion of electrons in a 2D system and second comes from the magnetic Brillouin zone. We have known that the magnetic Brillouin zone is $2q$ smaller than the orginal one. When magnetic field is turned on, we might obtained at least doublet degeneracy in Landau level. Second, in the absence of magnetic field, electron moving in periodic lattice crystal, but when a magnetic field is applied, electrons follow circular orbits (see in Fig. 2(a)). Here the Lorentz force are dominant, and the lattice potential is considered as slightly perturbation. Due to translational symmetry, these orbits can be positioned anywhere within the sample without changing their energy [5].

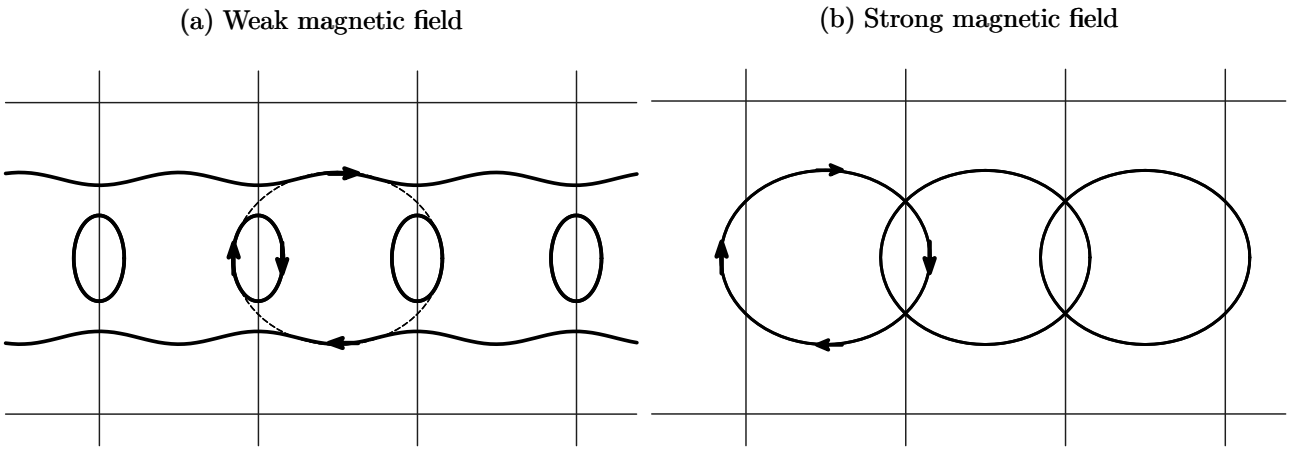

Figure 2: Periodic zone scheme, adapted from Kittel *et al.* [5]. The straight lines indicate the Brillouin zones, the curved lines in (a) represent the band structure, and the elliptical lines correspond to the cyclotron orbits.

When diagonalizing the Hamiltonian in Eq. (14), we obtain $2q$ eigenvalues for each

orbital $\phi_j(\mathbf{r})$, with $j = 1, 2, 3$. In total, this gives $6q$ eigenvalues. The eigenvalues corresponding to the valence band range from 1 to $2q$, while those of the conduction band range from $2q + 1$ to $4q$.

For instance, in Fig. 3(a), the first Landau level is labeled as $|0, 0\rangle_{K'}$. This level is degenerate, i.e., $E_{2q+1} = E_{2q+2}$, corresponding to the same energy value. Similarly, the second Landau level is labeled as $|0, 1\rangle_{K'}$, which corresponds to the two degenerate eigenvalues $E_{2q+3} = E_{2q+4}$, and so on for the subsequent Landau levels. In Fig. 3(e), for the valence band, we clearly observe the evidence of the Brillouin zone shrinking. At a given value of B, the energy value is obtained simultaneously at the K, K' and Γ points. The first Landau level in the valence band corresponds to the eigenvalue E_{2q} (labeled as $|0, 0\rangle_{\Gamma}$), which is degenerate with E_{2q-1}. The second Landau level then corresponds to E_{2q-2} and E_{2q-3}, and so on for the lower levels.

In terms of Eq. (18), we have

$$m_e^* = \frac{eB\hbar}{E_{2q+3} - E_{2q+1}}. \tag{30}$$

However, for m_h^*, the situation is quite different and more complicated than for m_e^*. For some cases, like MoS_2, this difficulty arises because the energy of the Γ point lies close to the K and K' valleys. As a consequence, in Fig. 1(d), the eigenvalues are no longer linear or follow the sequential index $2q - n$ as in the case of m_e^*, but instead exhibit level crossings due to numerical issues. To address this, first, we need to determine the energy value E_n at a given B that corresponds to the envelope function. This can be done by plotting all the wave functions from 0 to $2q$, since each wave function provides information about the Landau level labeling. From the wave functions, we can then identify which E_n corresponds to $|j, n\rangle_{\tau}$.

3 Numerical results

3.1 Effective mass

Monolayer MoS_2

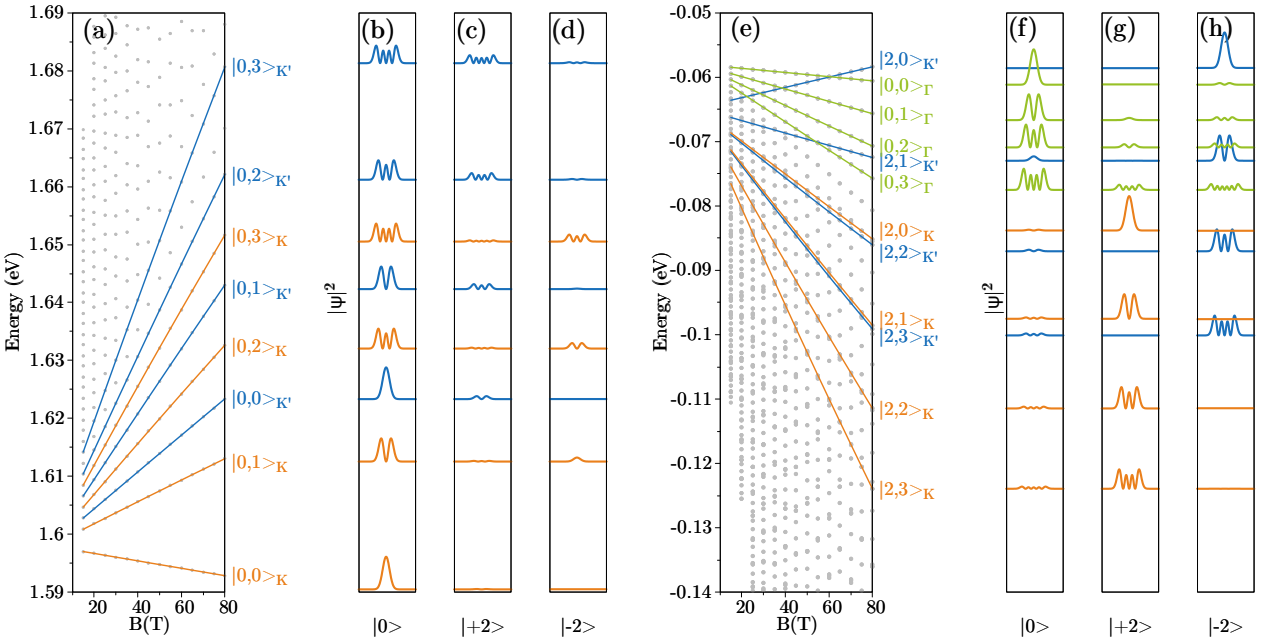

Figure 3: Landau levels (a) and the corresponding envelope-function components (b),(c),(d) for conduction electrons at valleys K and K'. Figs (e)–(h) show the same as (a)–(d) but for valence electrons. (Recalculated from Ho *et al.* [4])

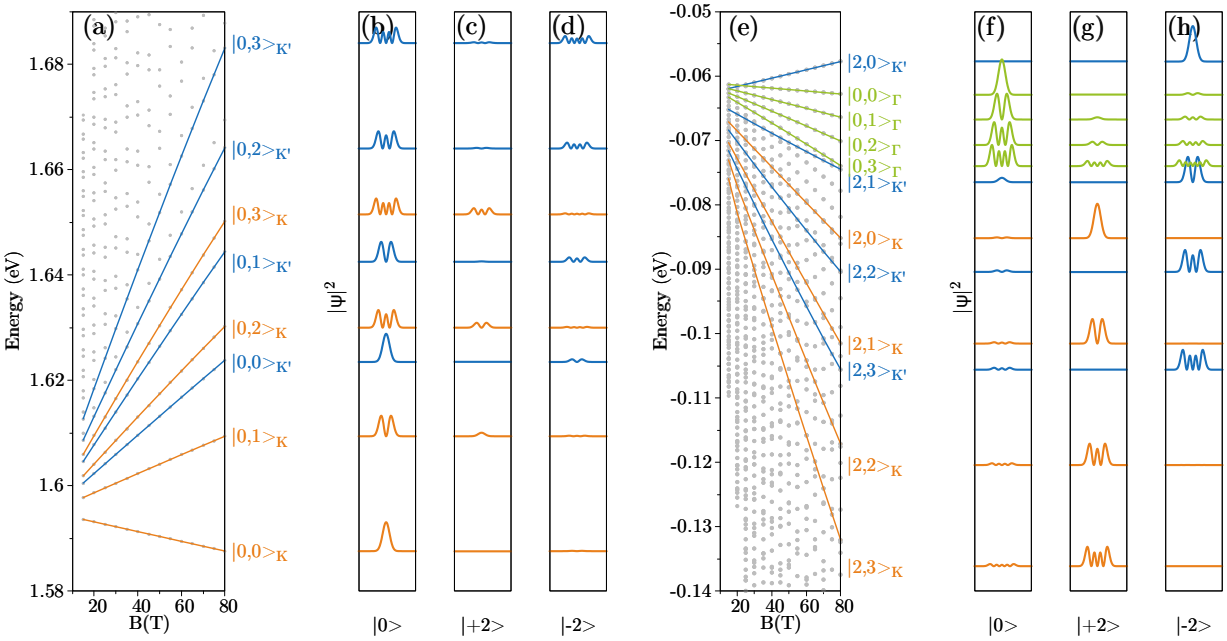

Figure 4: Same as Figure 1 but for TNN case.

The band structure of MoS_2 without a magnetic field shows that, in the valence band, the Γ point has an energy level of $E \approx -0.058$ eV. Therefore, when a magnetic

field is applied, this Γ-point energy level still appears. The Landau levels in conduction band are mainly contributed by the basis $|0\rangle$. In the valence band, the Γ, K, and K' points can be easily identified by their weights in the wavefunction. However, the situation is opposite in the conduction band. In this work, we adopt the results from the previous studies by Have *et al.* and Kormányos *et al.* [1, 6]. They shown that, in the conduction band the lowest Landau level is in valley K, while in valence band it is in valley K'.

The effective masses of MoS_2 in the absence of a magnetic field, calculated from

$$\frac{1}{m^*_{ij}} = \frac{1}{\hbar^2}\frac{\partial^2 E(\mathbf{k})}{\partial k_i \partial k_j}, \tag{31}$$

are $m_e \approx 0.4178m_0$, $m_h \approx 0.5325m_0$, and $m_r \approx 0.2341$ for the TNN case, and $m_e \approx 0.4508m_0$, $m_h \approx 0.6487m_0$, and $m_r \approx 0.2659m_0$ for the NN case.

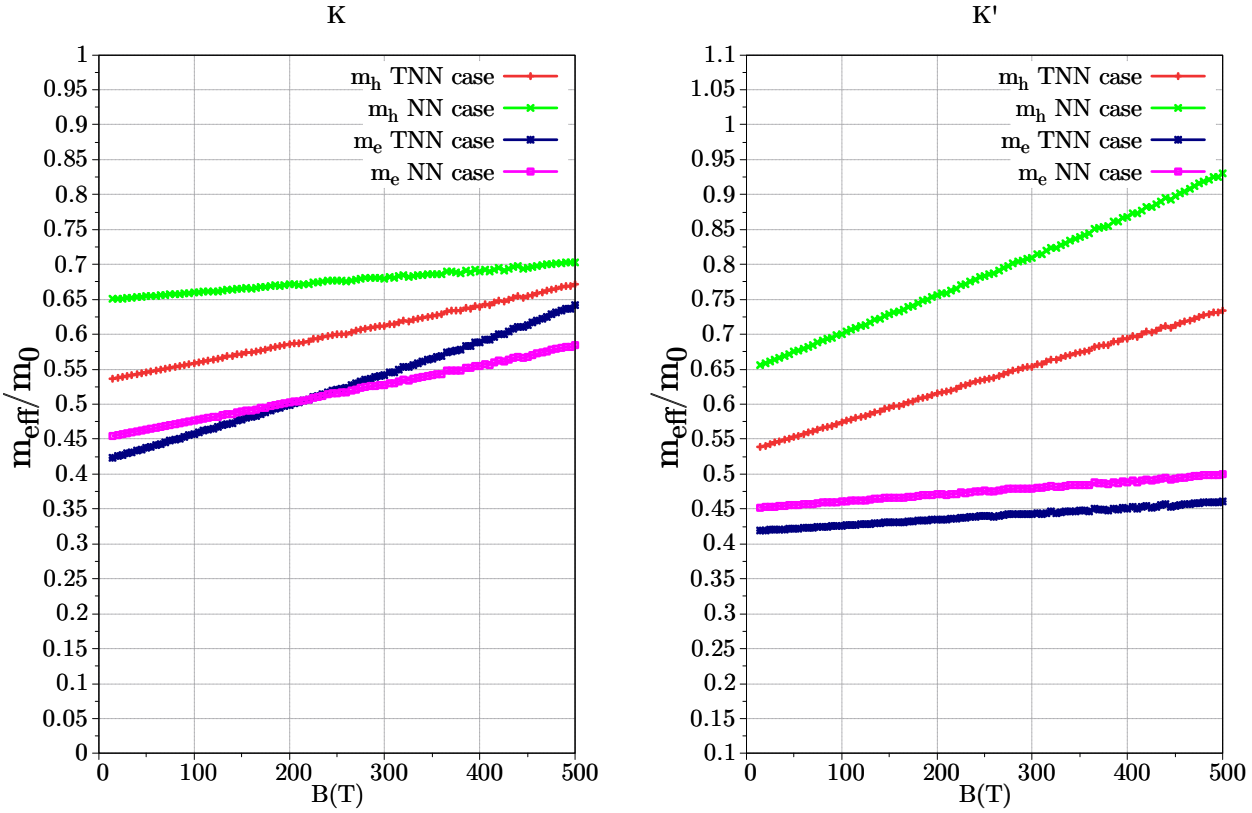

Figure 5: Effective masses.

When a strong magnetic field is applied, for example $B = 100$ T:

a) Nearest neighbor (NN)

- At valley K: $m_h \approx 0.7011m_0$, $m_e \approx 0.4763m_0$. The reduced mass is $m_r \approx 0.2836m_0$, which increases by $\approx 6.7\%$.
- At valley K': $m_h \approx 0.6597m_0$, $m_e \approx 0.4606m_0$. The reduced mass is $m_r \approx$

$0.2713m_0$, which increases by $\approx 2.0\%$.

b) Third nearest neighbor (TNN)

- At valley K: $m_h \approx 0.5739m_0$, $m_e \approx 0.4573m_0$. The reduced mass is $m_r \approx 0.2545m_0$, which increases by $\approx 8.71\%$.
- At valley K': $m_h \approx 0.5584m_0$, $m_e \approx 0.4263m_0$. The reduced mass is $m_r \approx 0.2417m_0$, which increases by $\approx 3.25\%$.

Meanwhile, Goryca *et al.* [7] reported that $m_r \approx 0.27 \pm 0.01m_0$, which is $4\% - 10.2\%$ larger than the earlier result of Berkelbach *et al.* [8], $m_r = 0.245 \pm 0.005m_0$. Based on our calculations, we argue that the reduced mass at valley K, $m_r \approx 0.2545m_0$ with an increase of 8.71%, is consistent with the experimental findings of Goryca *et al.*

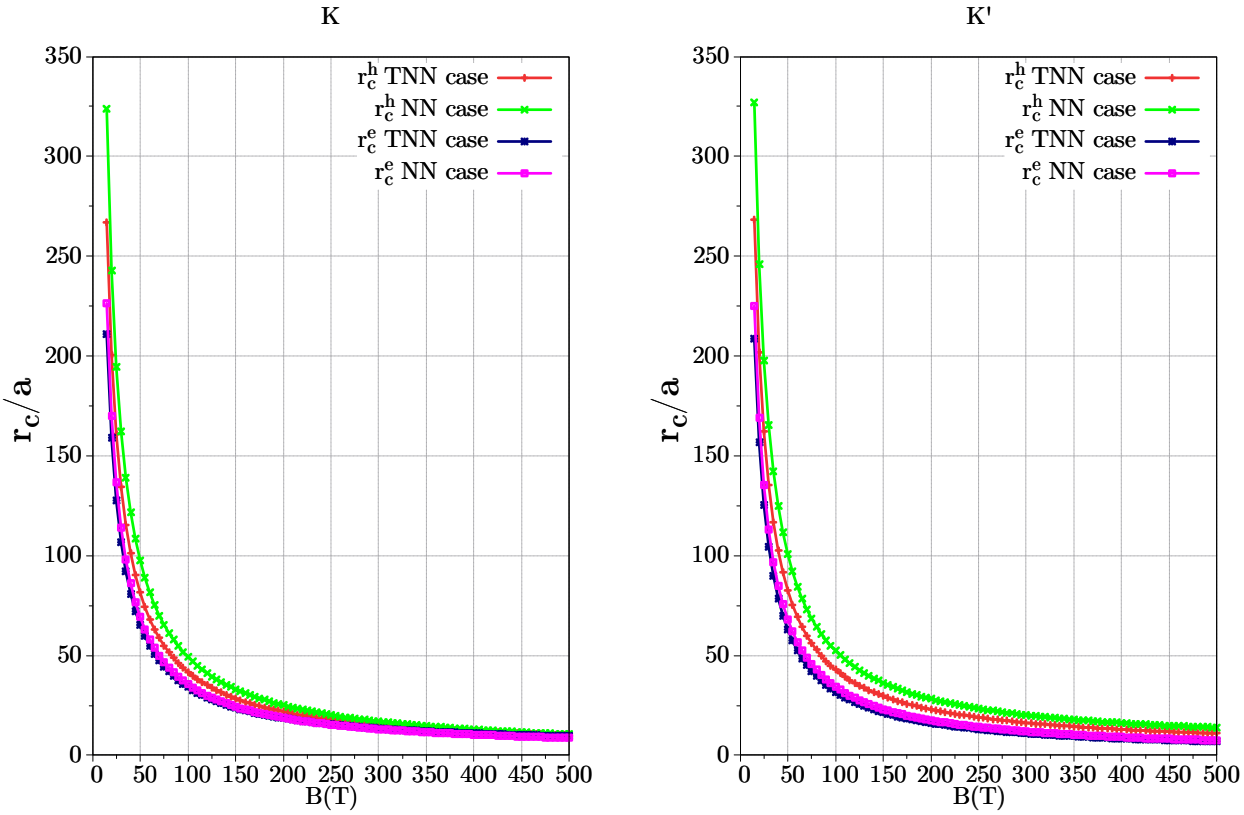

Figure 6: The ratio of the cyclotron radius r_c to the lattice constant a as a function of magnetic field B.

Monolayer $MoSe_2$

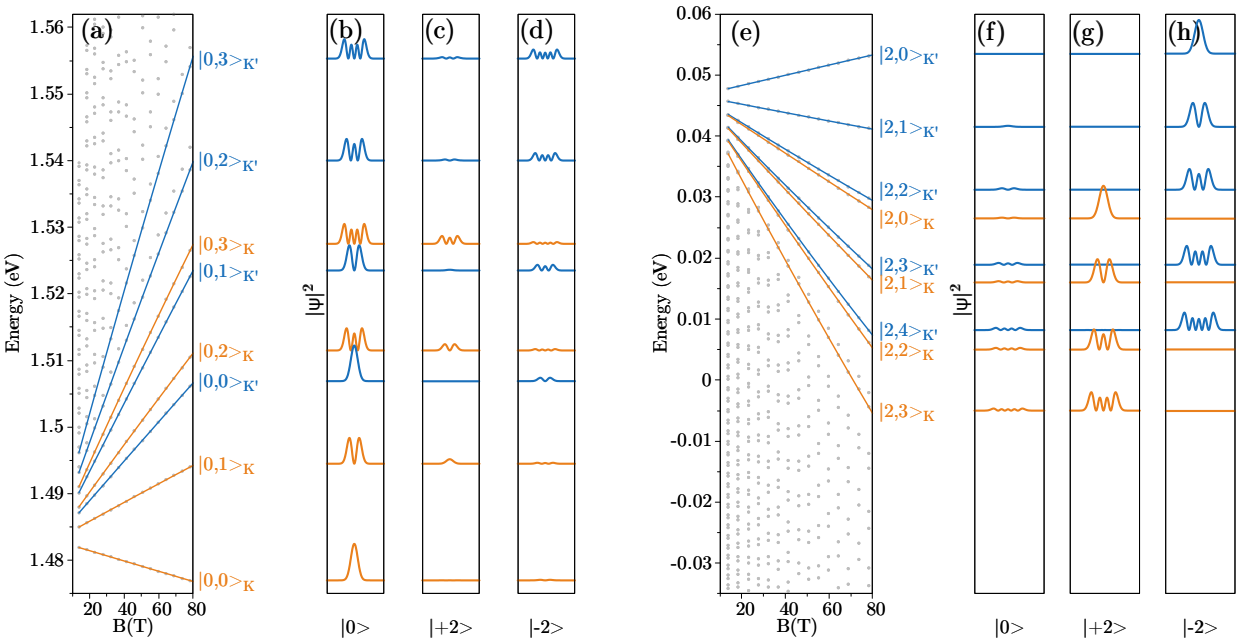

Figure 7: Landau levels (a) and the corresponding envelope-function components (b),(c) for conduction electrons at valleys K and K'. Figs (d)–(f) show the same as (a)–(c) but for valence electrons.

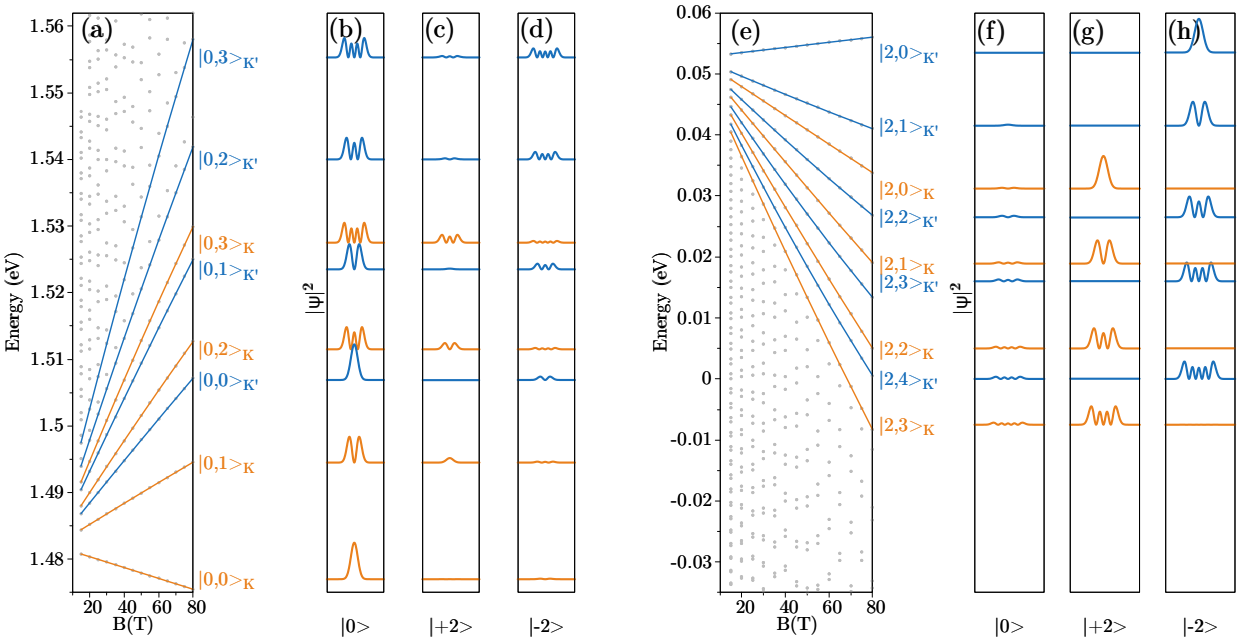

Figure 8: Same as Figure but for TNN case.

The band structure of $MoSe_2$ without a magnetic field shows that the Γ point does not appear near the K point. Therefore, when a magnetic field is applied, the Γ-point energy level is absent in this region. In addition, the first three Landau levels originate from the K' valley, in contrast to WSe_2, where the first two Landau levels originate from the K' valley.

The effective masses of $MoSe_2$ in the absence of a magnetic field, calculated from

$$\frac{1}{m^*_{ij}} = \frac{1}{\hbar^2}\frac{\partial^2 E(\mathbf{k})}{\partial k_i \partial k_j}, \tag{32}$$

are $m_e \approx 0.4770 m_0$, $m_h \approx 0.5887 m_0$, and $m_r \approx 0.2634 m_0$ for the TNN case, and $m_e \approx 0.5226 m_0$, $m_h \approx 0.7512 m_0$, and $m_r \approx 0.3082 m_0$ for the NN case.

When a strong magnetic field is applied, for example $B = 100$ T:

a) Nearest neighbor (NN)

- At valley K: $m_h \approx 0.8100 m_0$, $m_e \approx 0.5529 m_0$. The reduced mass is $m_r \approx 0.3286 m_0$, which increases by $\approx 6.62\%$.
- At valley K': $m_h \approx 0.7632 m_0$, $m_e \approx 0.5331 m_0$. The reduced mass is $m_r \approx 0.3138 m_0$, which increases by $\approx 1.82\%$.

b) Third nearest neighbor (TNN)

- At valley K: $m_h \approx 0.7168 m_0$, $m_e \approx 0.5320 m_0$. The reduced mass is $m_r \approx 0.3052 m_0$, which increases by $\approx 15.87\%$.
- At valley K': $m_h \approx 0.6251 m_0$, $m_e \approx 0.4874 m_0$. The reduced mass is $m_r \approx 0.2738 m_0$, which increases by $\approx 3.95\%$.

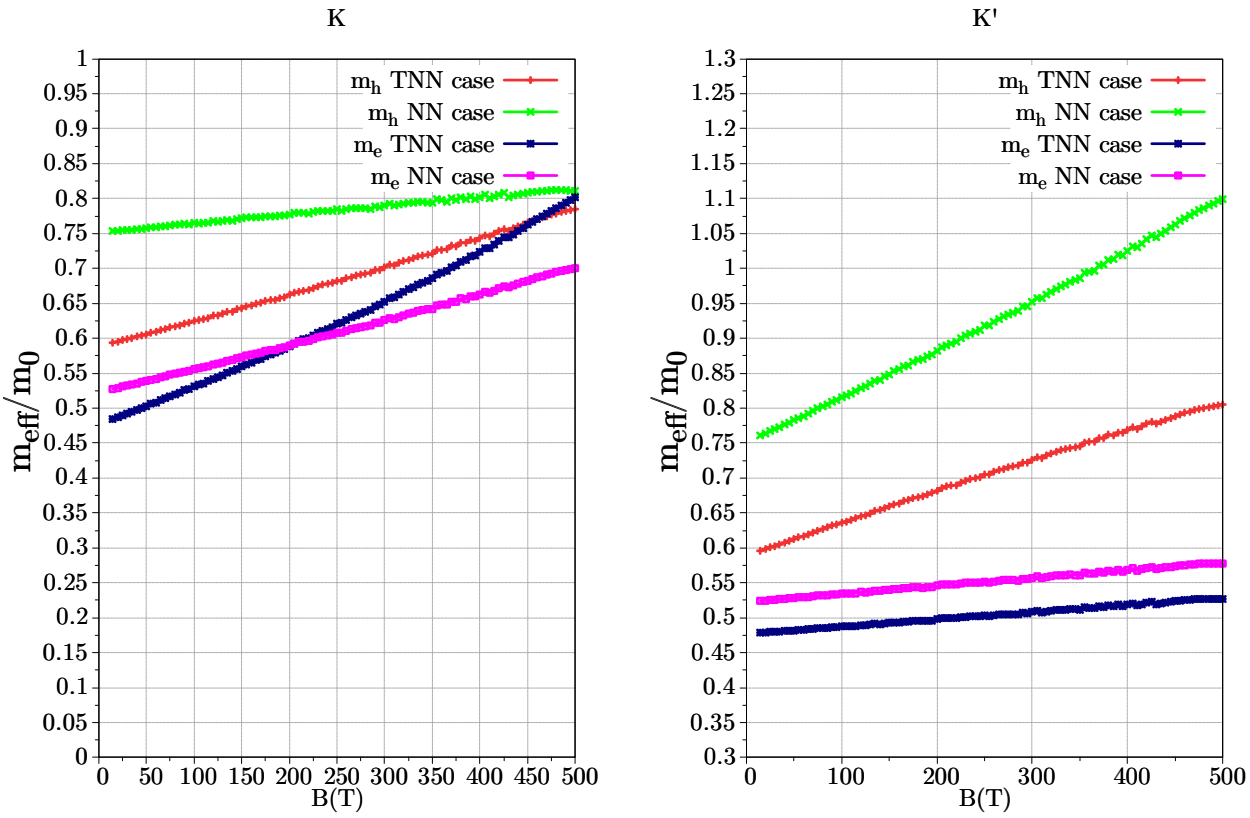

Figure 9: Effective masses.

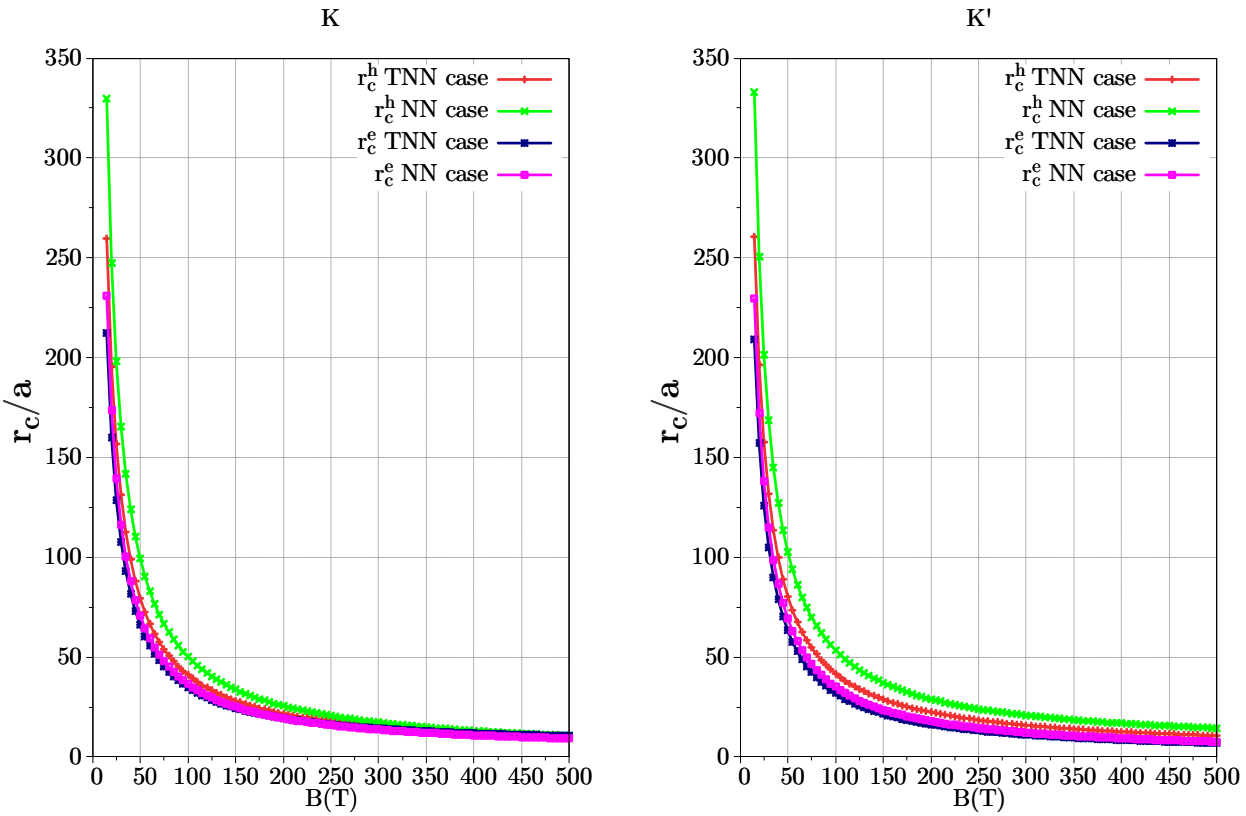

Figure 10: The ratio of the cyclotron radius r_c to the lattice constant a as a function of magnetic field B.

Meanwhile, Goryca *et al.* [7] reported that $m_r \approx 0.350 \pm 0.015 m_0$, which is $24.1\% - 35.2\%$ larger than the earlier result of Berkelbach *et al.* [8], $m_r = 0.27 m_0$. Based on our calculations, we argue that at valley K, the reduced mass $m_r \approx 0.3052 m_0$, with an increase of 15.87%, does not fully agree with the experimental findings of Goryca *et al.*.

Monolayer $MoTe_2$

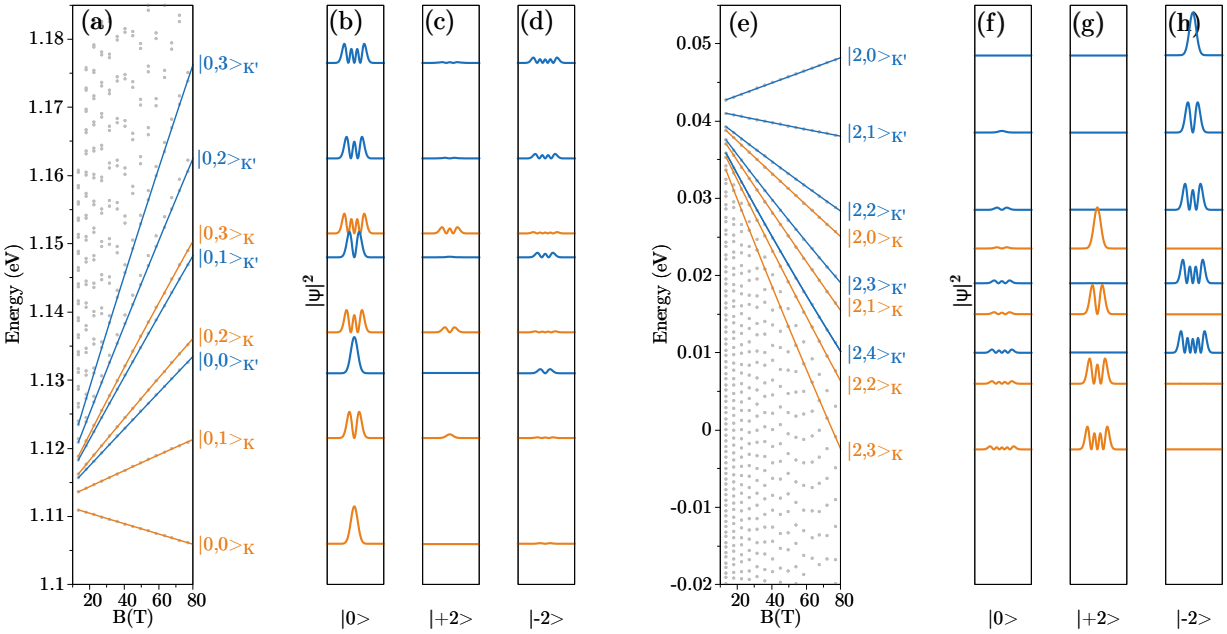

Figure 11: Landau levels (a) and the corresponding envelope-function components (b),(c) for conduction electrons at valleys K and K'. Figs (d)–(f) show the same as (a)–(c) but for valence electrons.

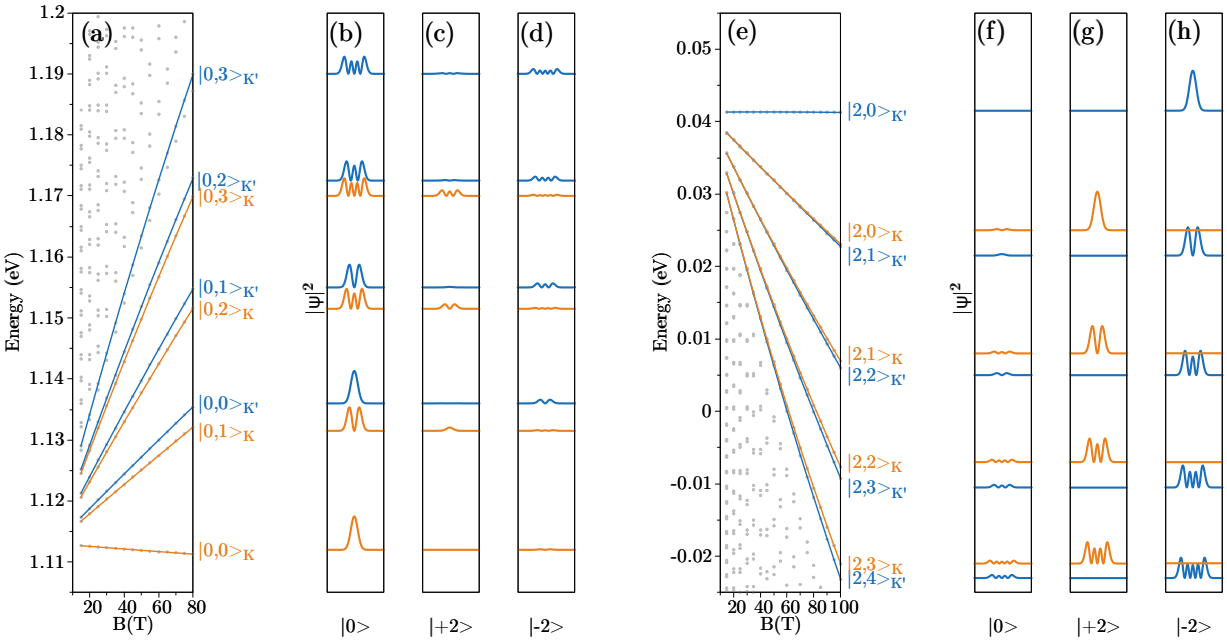

Figure 12: Landau levels (a) and the corresponding envelope-function components (b),(c) for conduction electrons at valleys K and K'. Figs (d)–(f) show the same as (a)–(c) but for valence electrons.

The band structure of $MoTe_2$ without a magnetic field shows that the Γ point has an energy level of $E \approx -0.1075$ eV. Therefore, when a magnetic field is applied, this Γ-point energy level not appears.

The effective masses of $MoTe_2$ in the absence of a magnetic field, calculated from

$$\frac{1}{m^*_{ij}} = \frac{1}{\hbar^2}\frac{\partial^2 E(\mathbf{k})}{\partial k_i \partial k_j}, \tag{33}$$

are $m_e \approx 0.4318m_0$, $m_h \approx 0.6044m_0$, and $m_r \approx 0.2519m_0$ for the TNN case, and $m_e \approx 0.5913m_0$, $m_h \approx 0.8975m_0$, and $m_r \approx 0.3565m_0$ for the NN case, as also reported by Goryca *et al.* [7]. Among the six materials considered, $MoTe_2$ has the largest effective masses m_e and m_h in the absence of a magnetic field.

When a strong magnetic field is applied, for example $B = 90$ T:

a) Nearest neighbor (NN)

- At valley K: $m_h \approx 0.9774m_0$, $m_e \approx 0.6304m_0$. The reduced mass is $m_r \approx 0.3832m_0$, which increases by $\approx 7.49\%$.
- At valley K': $m_h \approx 0.9142m_0$, $m_e \approx 0.6034m_0$. The reduced mass is $m_r \approx 0.3635m_0$, which increases by $\approx 1.96\%$.

b) Third nearest neighbor (TNN)

- At valley K: $m_h \approx 0.7704m_0$, $m_e \approx 0.4850m_0$. The reduced mass is $m_r \approx 0.2976m_0$, which increases by $\approx 18.14\%$.
- At valley K': $m_h \approx 0.6322m_0$, $m_e \approx 0.4463m_0$. The reduced mass is $m_r \approx 0.2616m_0$, which increases by $\approx 3.85\%$.

In the study of Goryca *et al.* [7], the reduced mass was reported as $m_r = 0.36 \pm 0.04m_0$, which is about 25% larger than the value obtained in the work of Kormányos *et al.* [9]. In our case, for the TNN model, the reduced mass is $m_r = 0.2976m_0$, which increases by $\approx 18\%$ compared to the zero-field value $m_r = 0.2519m_0$.

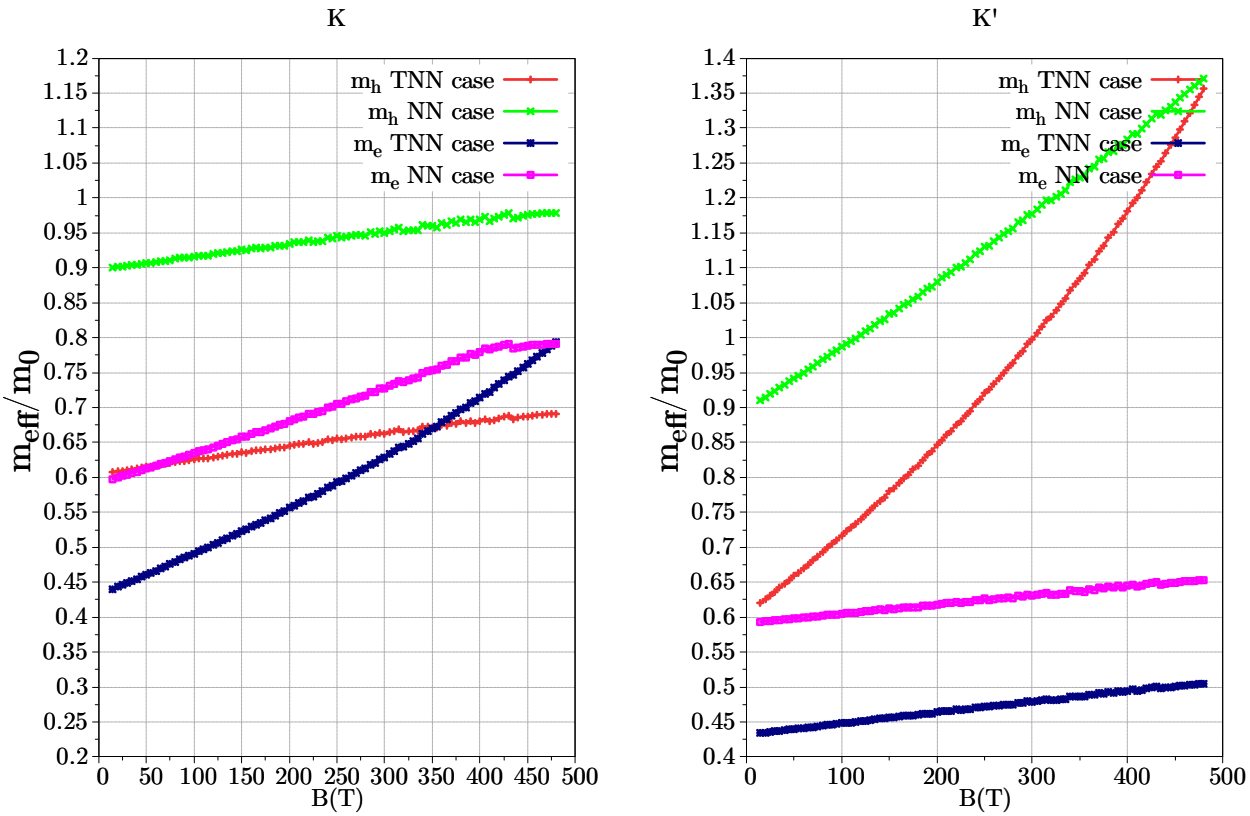

Figure 13: Effective masses.

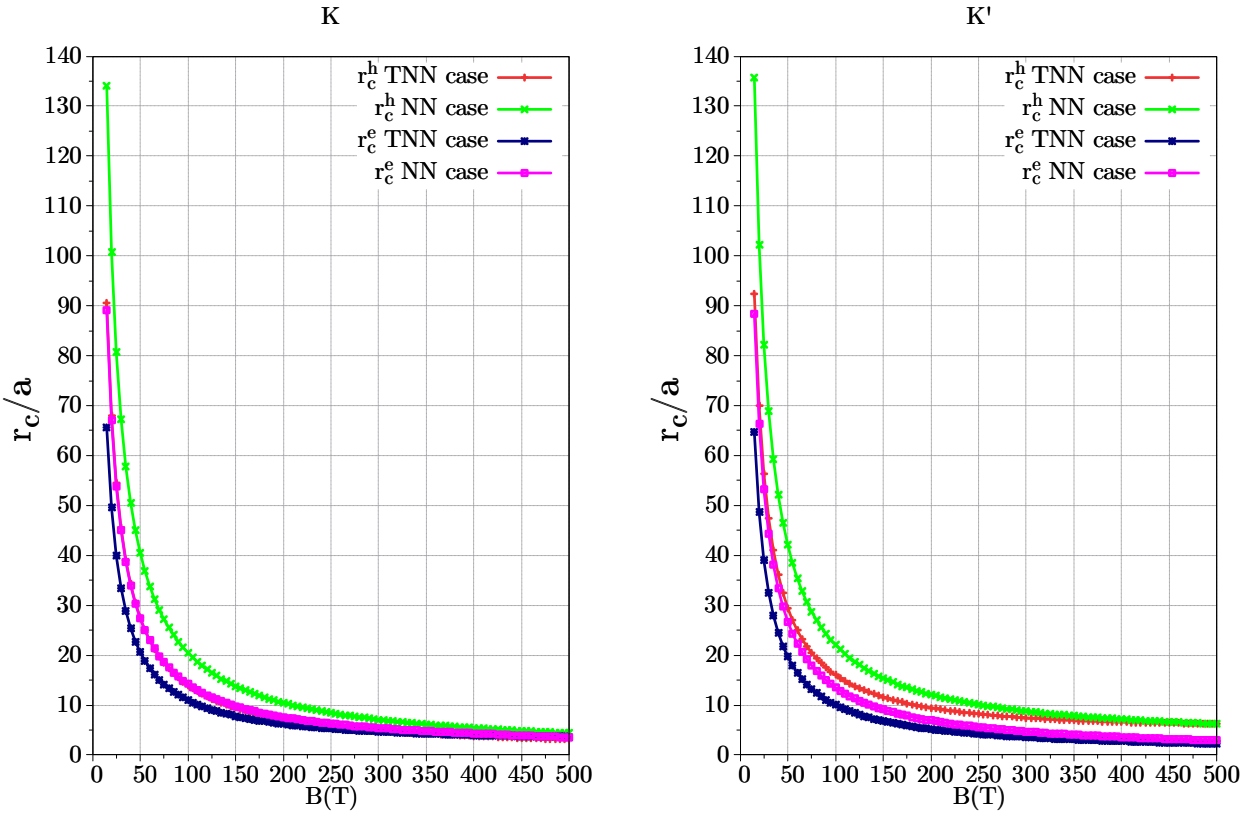

Figure 14: Effective masses.

Monolayer WS_2

The band structure of WS_2 without a magnetic field shows that the Γ point has an energy level of $E \approx -0.1075$ (eV). Therefore, when a magnetic field is applied, the

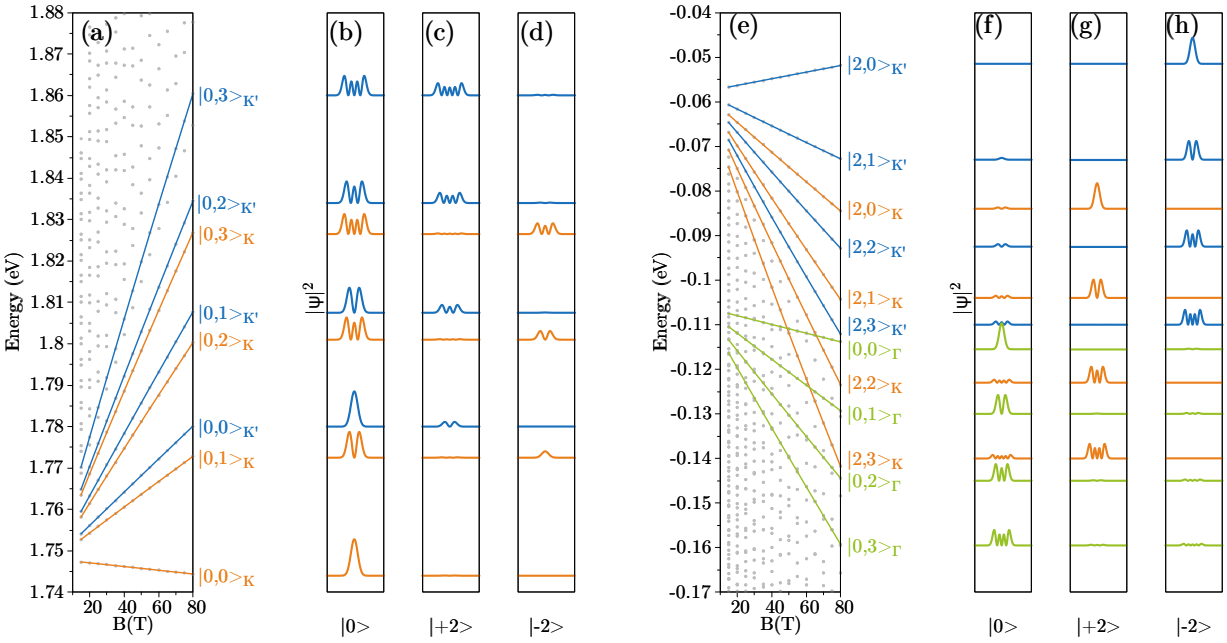

Figure 15: Landau levels (a) and the corresponding envelope-function components (b),(c) for conduction electrons at valleys K and K'. Figs (d)–(f) show the same as (a)–(c) but for valence electrons.

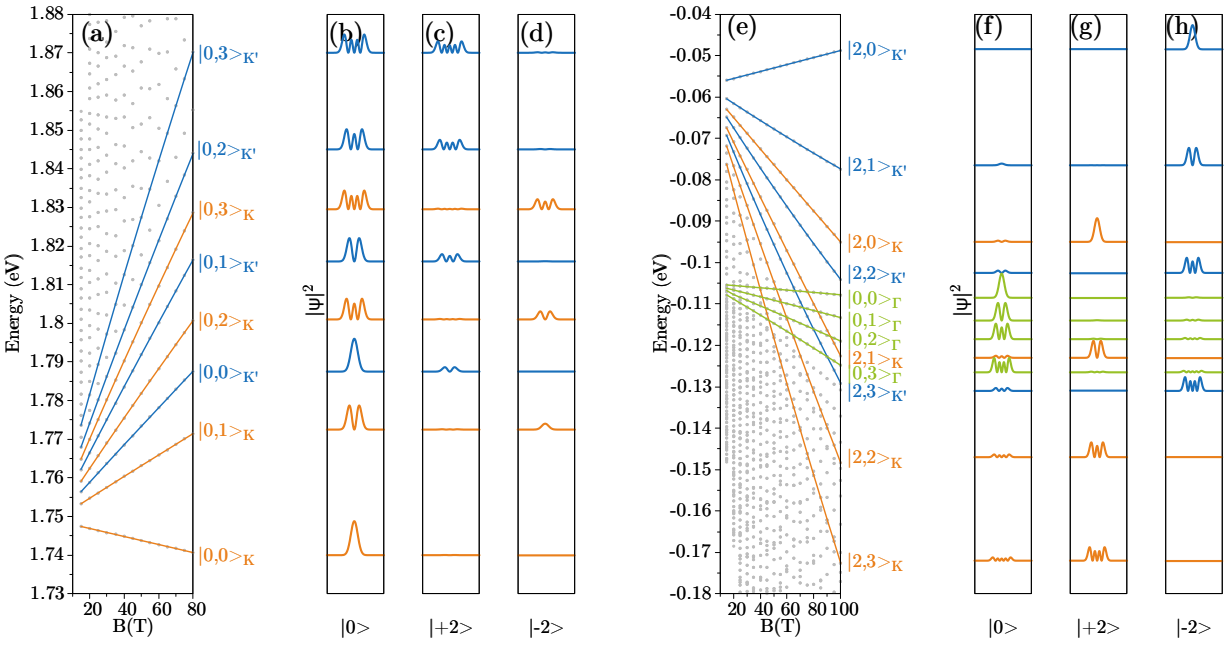

Figure 16: Landau levels (a) and the corresponding envelope-function components (b),(c) for conduction electrons at valleys K and K'. Figs (d)–(f) show the same as (a)–(c) but for valence electrons.

energy level at the Γ point still appears.

The effective mass of WS_2 without a magnetic field, calculated using

$$\frac{1}{m^*_{ij}} = \frac{1}{\hbar^2}\frac{\partial^2 E(\mathbf{k})}{\partial k_i k_j}, \tag{34}$$

yields $m_e \approx 0.2956 m_0$, $m_h \approx 0.3845 m_0$, $m_r \approx 0.1671 m_0$ in the TNN case, and $m_e \approx$

$0.3195m_0$, $m_h \approx 0.4348m_0$, $m_r \approx 0.1841m_0$ in the NN case.

For a strong magnetic field, e.g., $B = 100$ T:

a) Nearest neighbor

- At the K valley: $m_h \approx 0.4735m_0$, $m_e \approx 0.3389m_0$. Thus, $m_r \approx 0.1974m_0$, which increases by $\approx 7.2\%$.
- At the K' valley: $m_h \approx 0.4438m_0$, $m_e \approx 0.3273m_0$. Thus, $m_r \approx 0.1885m_0$, which increases by $\approx 2.3\%$.

b) Third nearest neighbor

- At the K valley: $m_h \approx 0.4205m_0$, $m_e \approx 0.3275m_0$. Thus, $m_r \approx 0.1841m_0$, which increases by $\approx 10.17\%$.
- At the K' valley: $m_h \approx 0.4043m_0$, $m_e \approx 0.3023m_0$. Thus, $m_r \approx 0.1730m_0$, which increases by $\approx 3.53\%$.

In the study of Goryca *et al.* [7], they reported $m_r = 0.175 \pm 0.007m_0$, which is about 10% larger than the value $m_r = 0.15 - 0.16m_0$ obtained in the work of Berkelbach *et al.* [8].

In our case, for the K valley under the TNN approximation, we obtain $m_r \approx 0.1841m_0$ in the presence of a magnetic field, which corresponds to an increase of $\approx 10\%$ compared to $m_r \approx 0.1671m_0$ without a magnetic field. This result is consistent with and reasonable compared to the experimental findings of Goryca *et al.* [7].

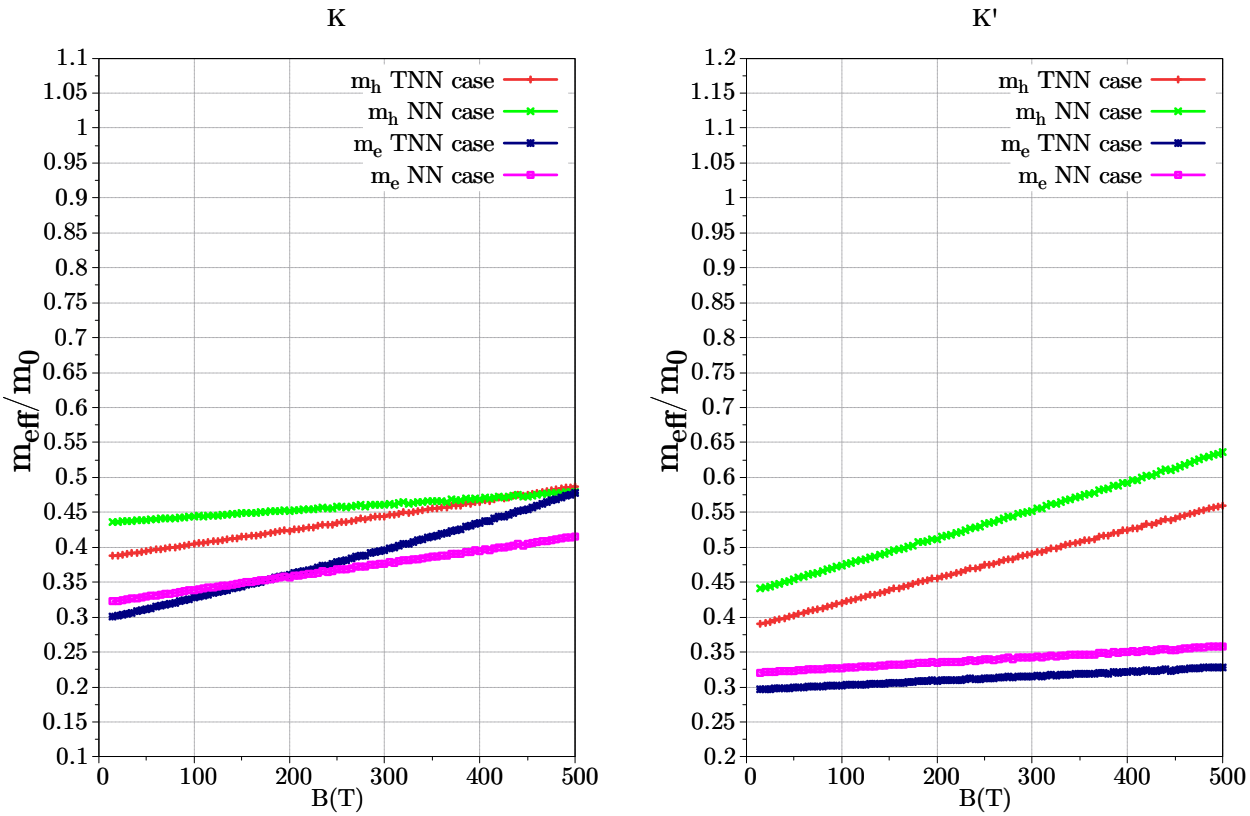

Figure 17: Mass.

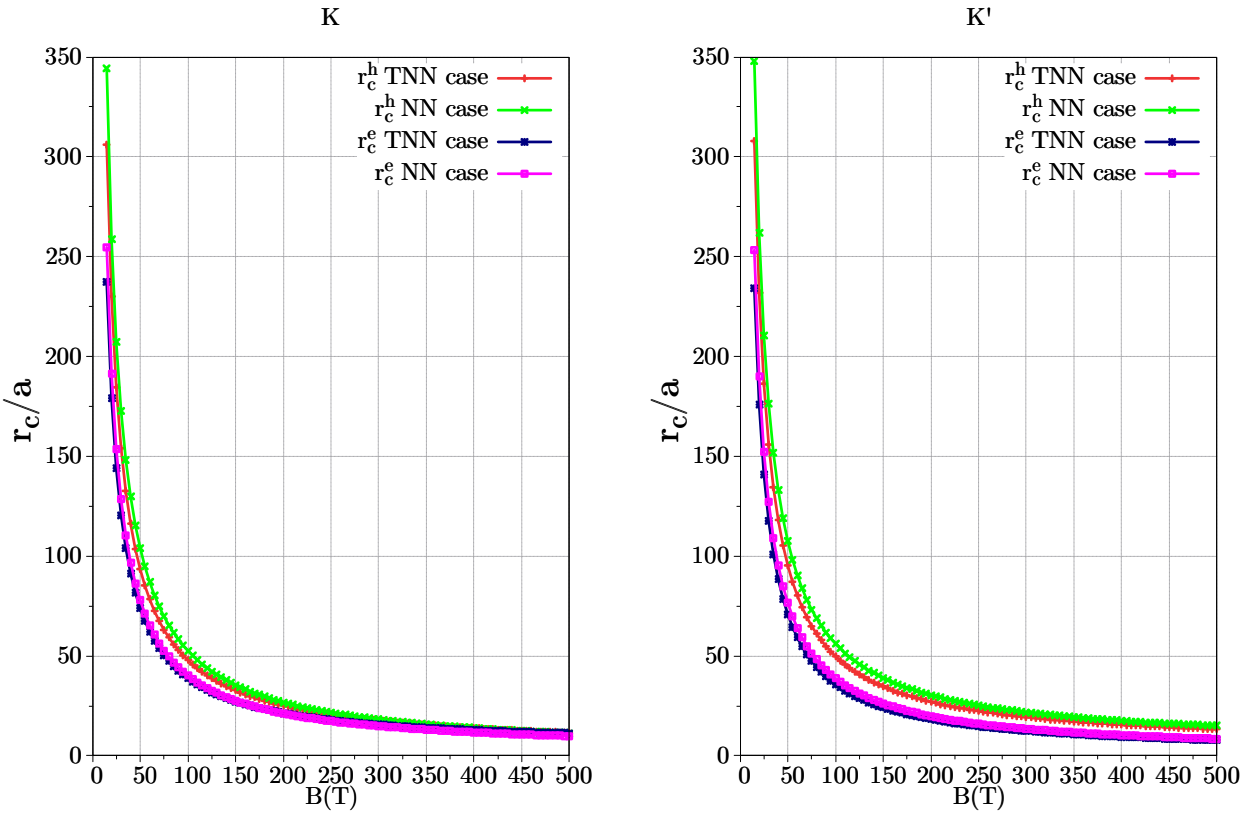

Figure 18: The ratio of the cyclotron radius r_c to the lattice constant a as a function of magnetic field B.

Monolayer WSe_2

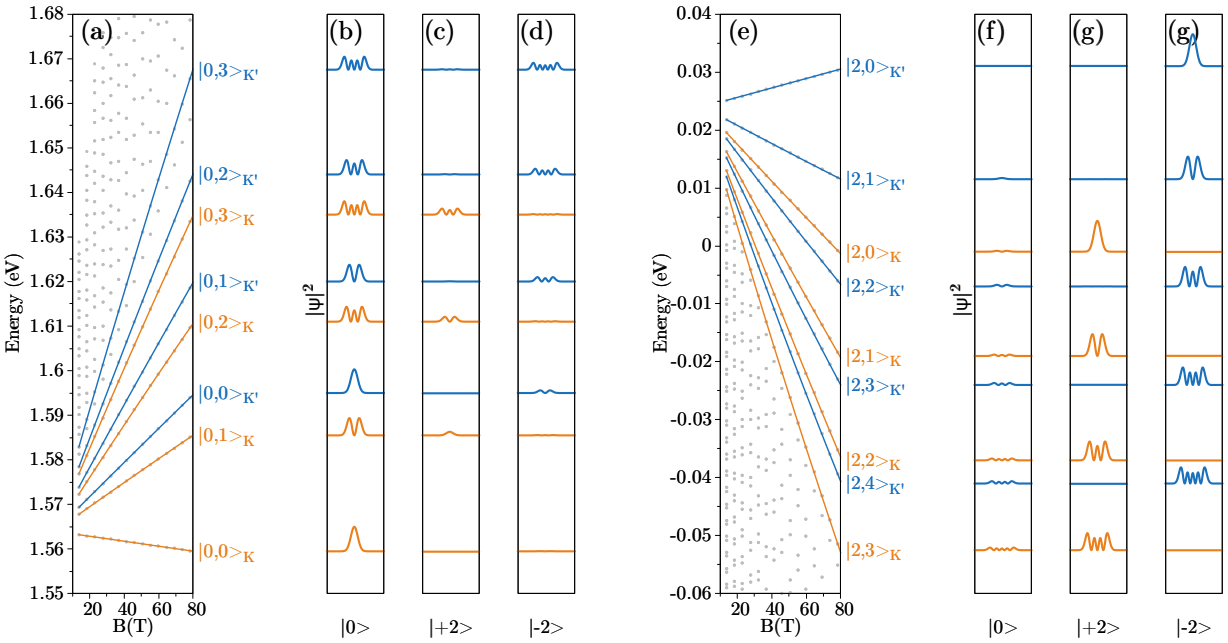

Figure 19: Landau levels (a) and the corresponding envelope-function components (b),(c) for conduction electrons at valleys K and K'. Figs (d)–(f) show the same as (a)–(c) but for valence electrons.

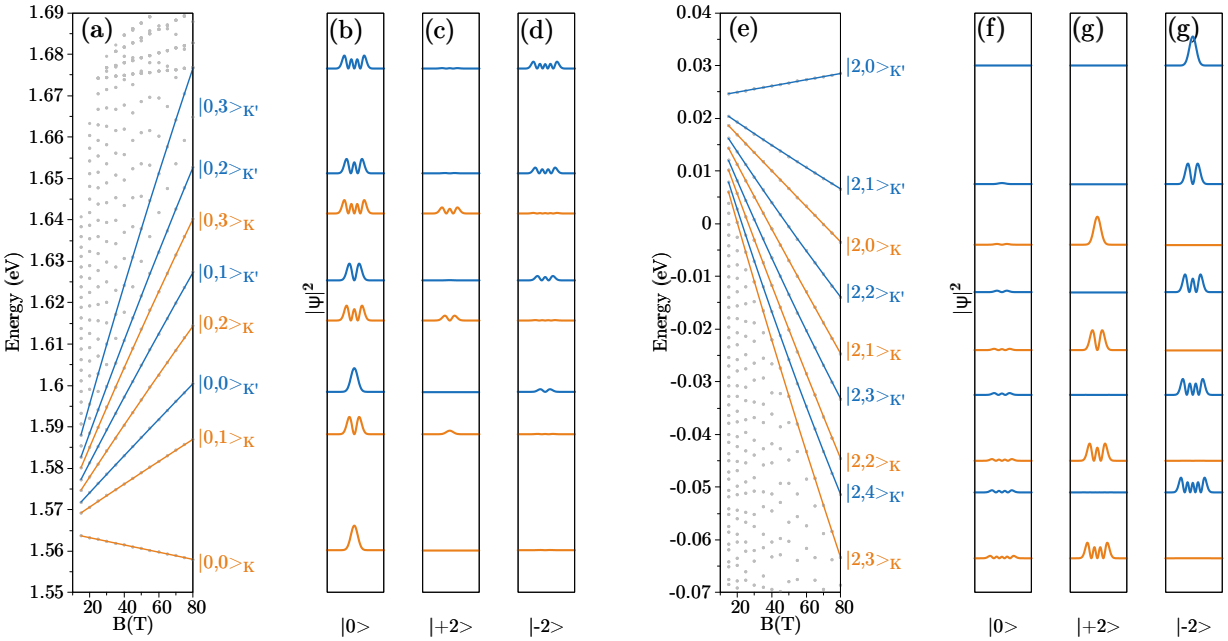

Figure 20: Landau levels (a) and the corresponding envelope-function components (b),(c) for conduction electrons at valleys K and K'. Figs (d)–(f) show the same as (a)–(c) but for valence electrons.

The band structure of WSe_2 without a magnetic field shows that the Γ point lies much lower in energy than the K point. Therefore, when a magnetic field is applied, the energy level at the Γ point does not appear here.

The effective mass of WSe_2 without a magnetic field, calculated using

$$\frac{1}{m_{ij}^*} = \frac{1}{\hbar^2}\frac{\partial^2 E(\mathbf{k})}{\partial k_i k_j}, \tag{35}$$

yields $m_e \approx 0.3124m_0$, $m_h \approx 0.4022m_0$, $m_r \approx 0.1758m_0$ in the TNN case, and $m_e \approx 0.3487m_0$, $m_h \approx 0.4792m_0$, $m_r \approx 0.2018m_0$ in the NN case, as reported in the works of Kylänpää *et al.* and Berkelbach *et al.* [8, 10].

For a strong magnetic field, e.g., $B = 100$ T:

a) Nearest neighbor

- At the K valley: $m_h \approx 0.5220m_0$, $m_e \approx 0.3702m_0$. Thus, $m_r \approx 0.2166m_0$, which increases by $\approx 7.34\%$.
- At the K' valley: $m_h \approx 0.4888m_0$, $m_e \approx 0.3573m_0$. Thus, $m_r \approx 0.2064m_0$, which increases by $\approx 2.28\%$.

b) Third nearest neighbor

- At the K valley: $m_h \approx 0.4417m_0$, $m_e \approx 0.3494m_0$. Thus, $m_r \approx 0.1951m_0$, which increases by $\approx 10.98\%$.
- At the K' valley: $m_h \approx 0.4257m_0$, $m_e \approx 0.3199m_0$. Thus, $m_r \approx 0.1826m_0$, which increases by $\approx 3.87\%$.

In the study of Stier *et al.* [11], they reported $m_r \approx 0.20 \pm 0.01m_0$, which is about 15% larger than the predictions of recent theoretical works [8, 10]. In our case, for the K valley under the TNN approximation, we obtain $m_r \approx 0.1951m_0$ in the presence of a magnetic field, corresponding to an increase of $\approx 11\%$ compared to the value without a magnetic field. This result is consistent with the findings reported by Stier *et al.* [11].

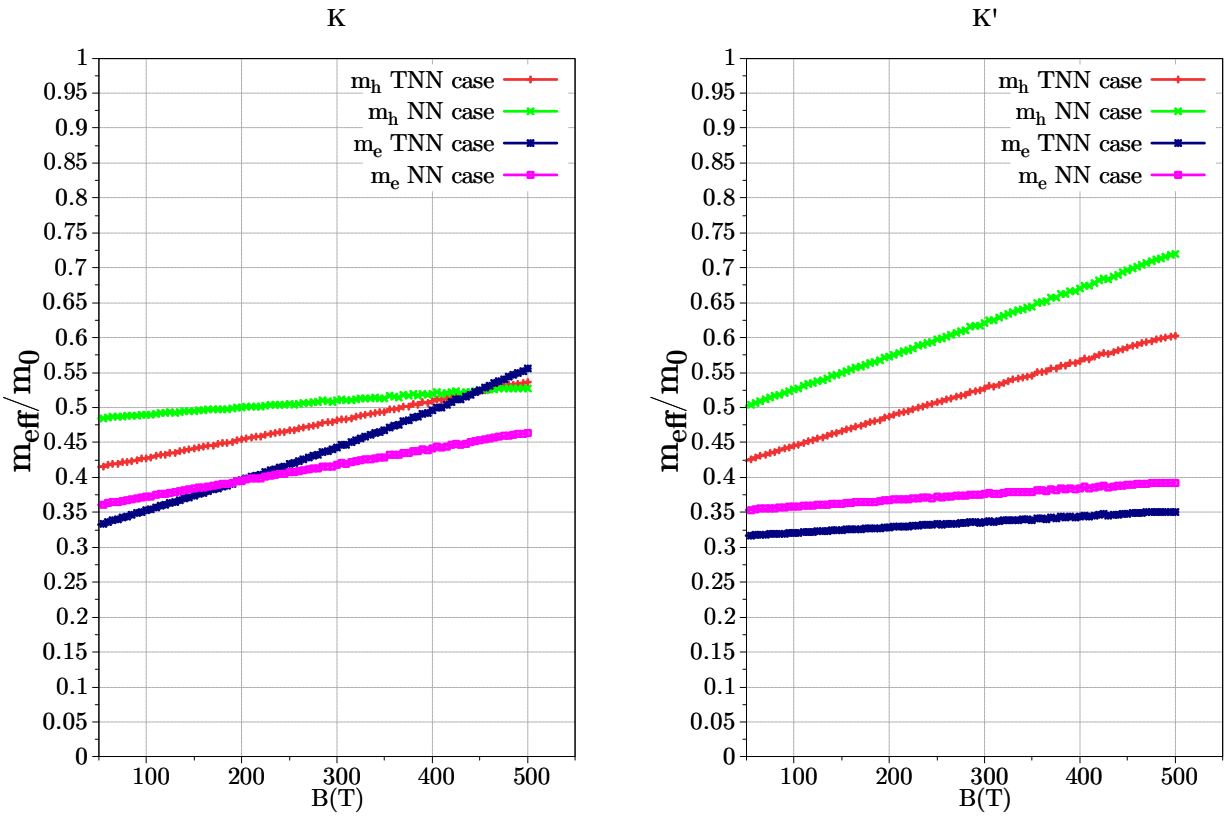

Figure 21: Mass.

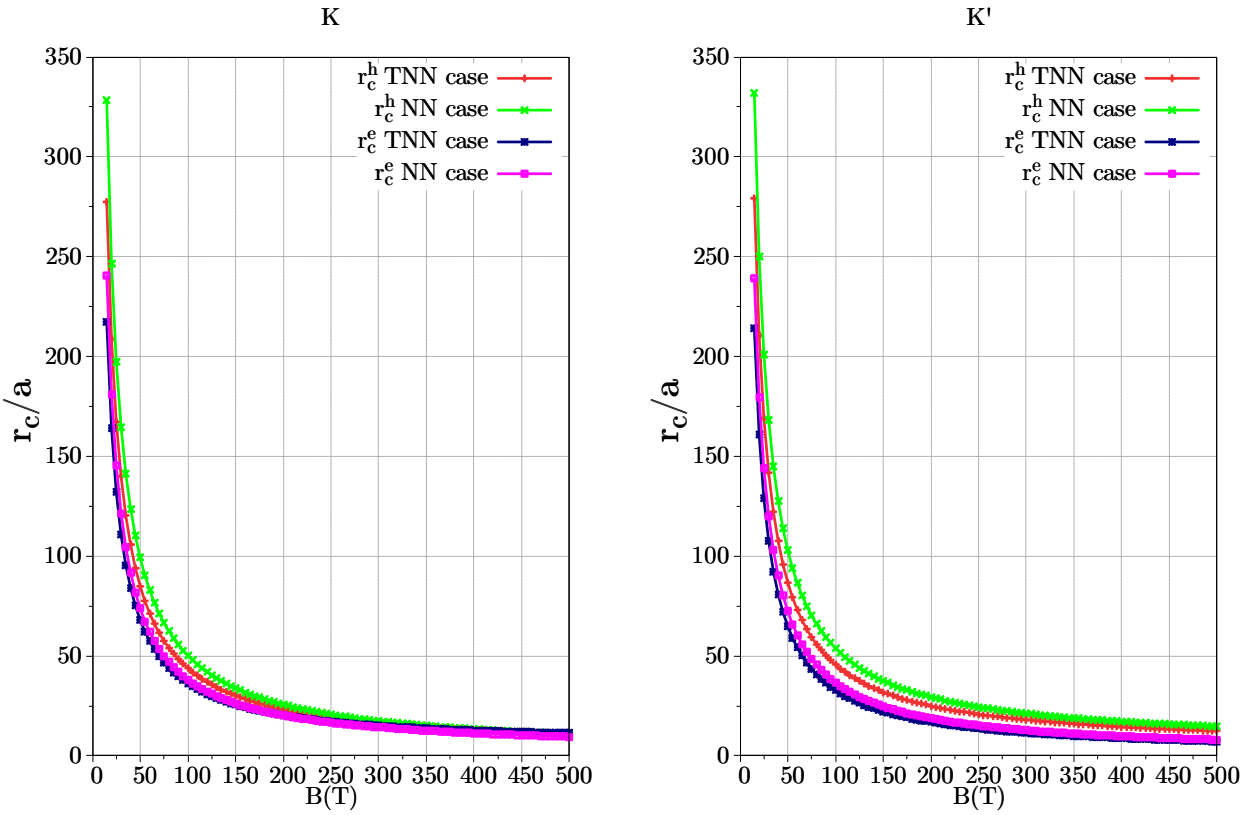

Figure 22: The ratio of the cyclotron radius r_c to the lattice constant a as a function of magnetic field B.

Monolayer WTe_2

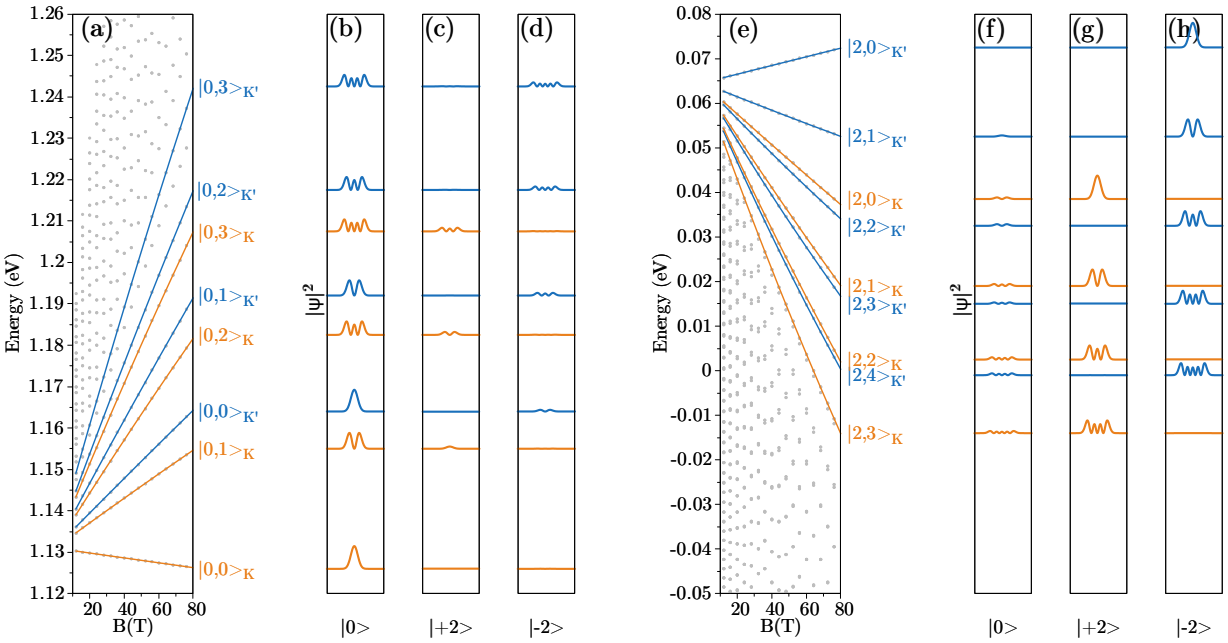

Figure 23: Landau levels (a) and the corresponding envelope-function components (b),(c) for conduction electrons at valleys K and K'. Figs (d)–(f) show the same as (a)–(c) but for valence electrons.

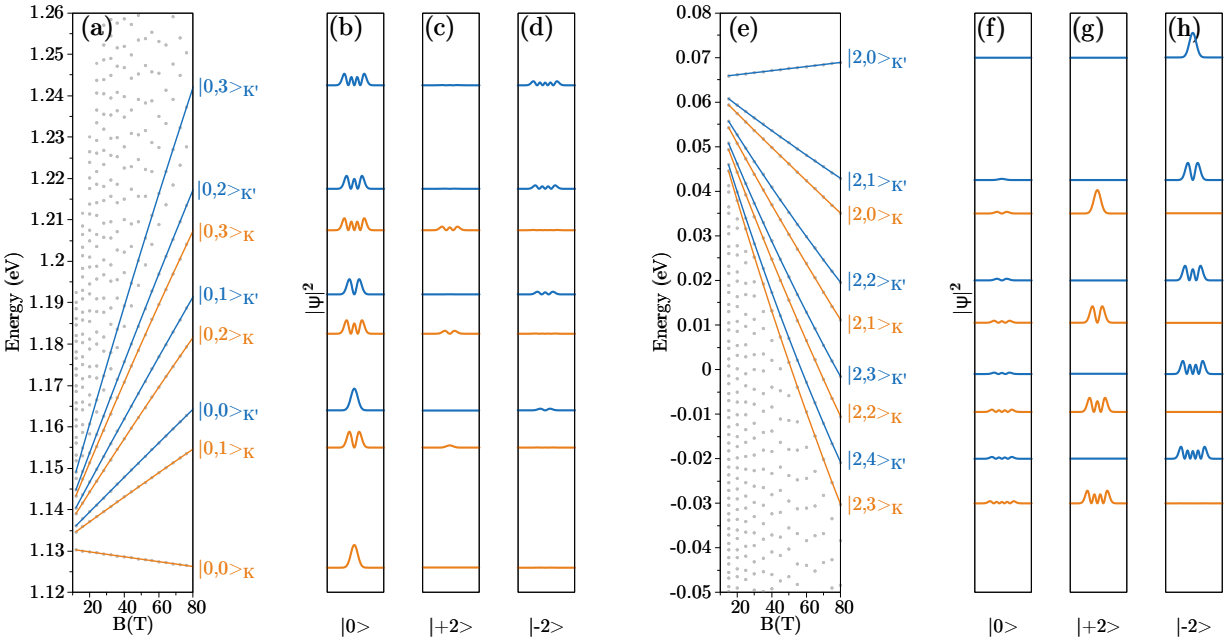

Figure 24: Landau levels (a) and the corresponding envelope-function components (b),(c) for conduction electrons at valleys K and K'. Figs (d)–(f) show the same as (a)–(c) but for valence electrons.

The band structure of WTe_2 in the absence of a magnetic field shows that the Γ point lies significantly lower in energy than the K point. Therefore, under an applied magnetic field, the Landau levels associated with the Γ point do not appear in this regime.

The effective masses of WTe_2 without a magnetic field, calculated using the formula

$$\frac{1}{m^*_{ij}} = \frac{1}{\hbar^2}\frac{\partial^2 E(\mathbf{k})}{\partial k_i k_j}, \tag{36}$$

are found to be $m_e \approx 0.2478m_0$, $m_h \approx 0.3332m_0$, and $m_r \approx 0.1421m_0$ for the TNN case, and $m_e \approx 0.3169m_0$, $m_h \approx 0.4559m_0$, and $m_r \approx 0.187m_0$ for the NN case. To the best of our knowledge, no previous studies have reported the effective masses of WTe_2.

At a high magnetic field, for example $B = 80$ T, the effective masses are obtained as follows:

a) Nearest neighbor

- At the K valley: $m_h \approx 0.5093m_0,\ m_e \approx 0.3413m_0$.
  This yields $m_r \approx 0.2044m_0$, corresponding to an increase of $\approx 9.3\%$.
- At the K′ valley: $m_h \approx 0.4681m_0,\ m_e \approx 0.3264m_0$.
  This gives $m_r \approx 0.1923m_0$, corresponding to an increase of $\approx 2.83\%$.

b) Third nearest neighbor

- At the K valley: $m_h \approx 0.387m_0,\ m_e \approx 0.2824m_0$.
  This yields $m_r \approx 0.1633m_0$, corresponding to an increase of $\approx 14.92\%$.
- At the K′ valley: $m_h \approx 0.3562m_0,\ m_e \approx 0.2577m_0$.
  This gives $m_r \approx 0.1495m_0$, corresponding to an increase of $\approx 5.21\%$.

Thus, at the K valley in the TNN case, the reduced mass m_r of WTe_2 exhibits an increasing of nearly 15% under a strong magnetic field, which is consistent with the trend observed for other materials discussed above.

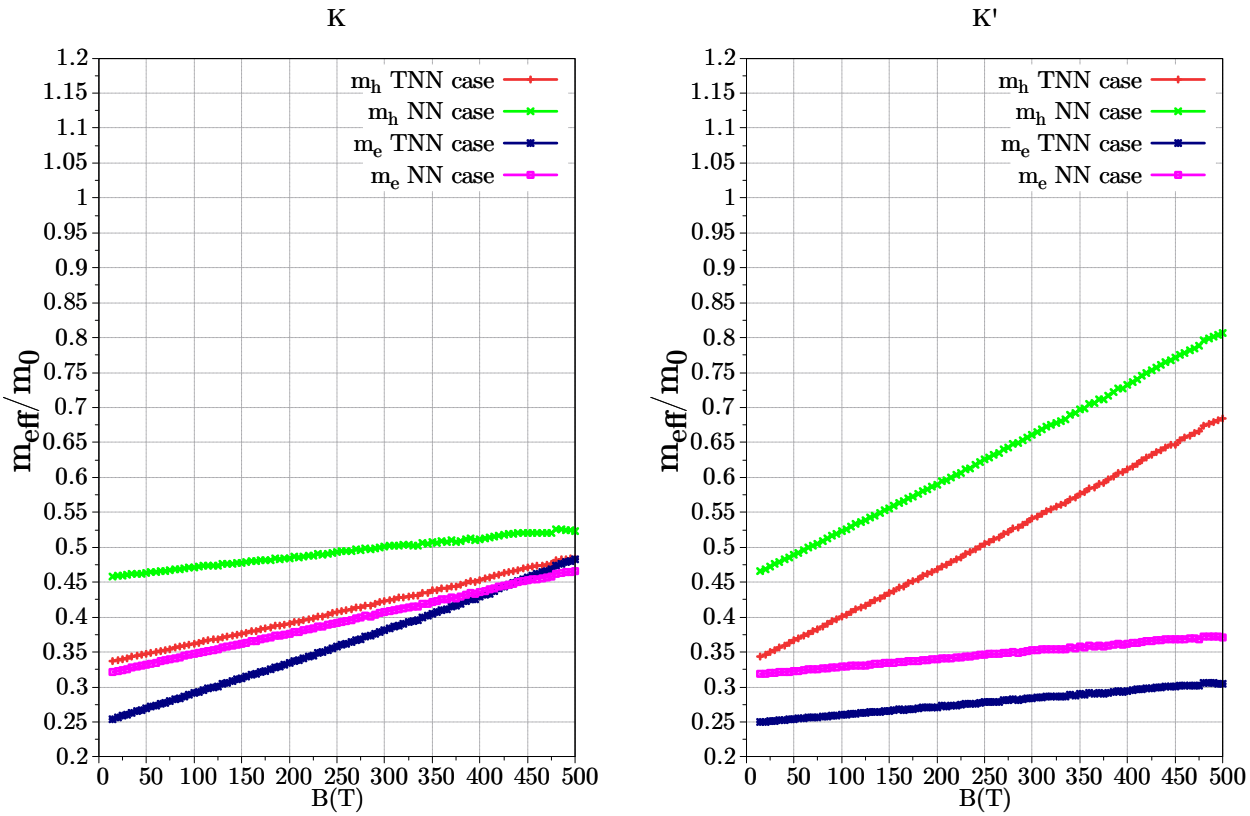

Figure 25: Mass.

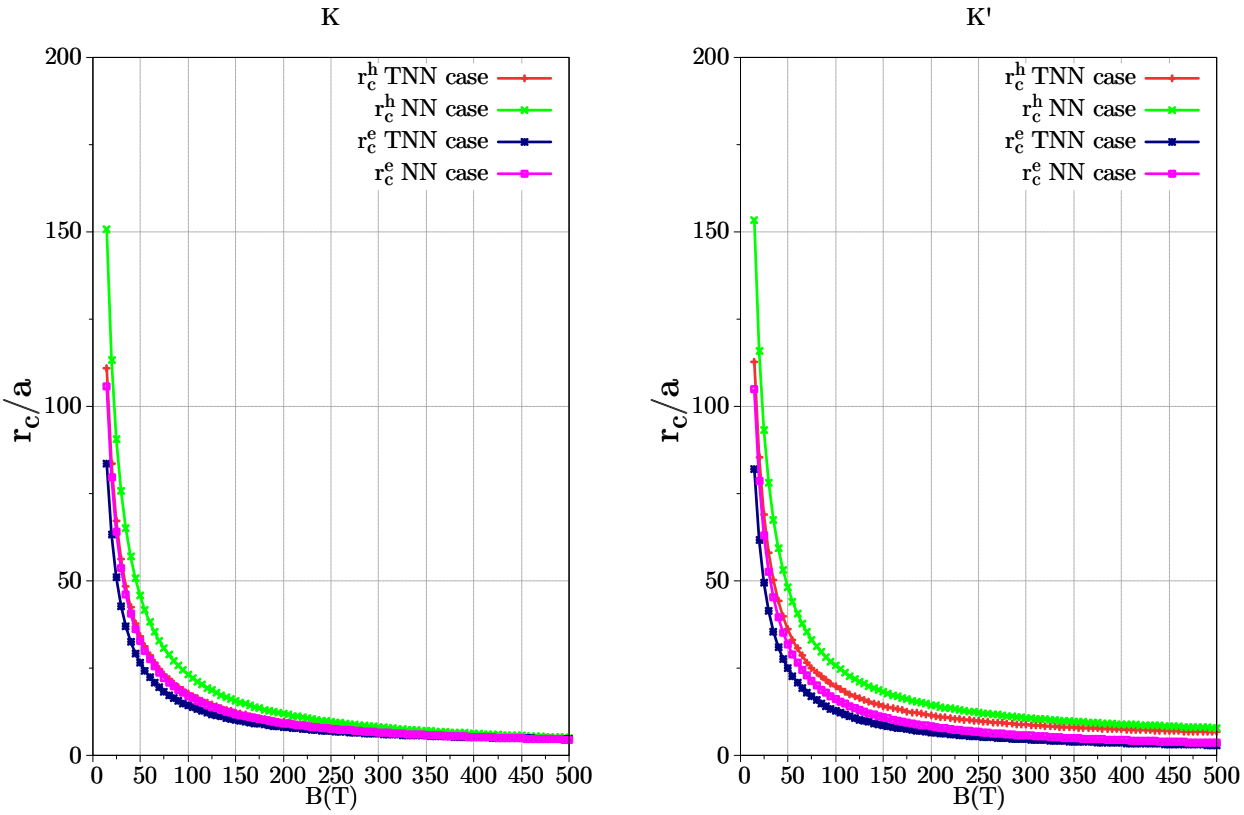

Figure 26: The ratio of the cyclotron radius r_c to the lattice constant a as a function of magnetic field B.

References

[1] Jonas Have, G Catarina, Thomas Garm Pedersen, and NMR Peres. Monolayer transition metal dichalcogenides in strong magnetic fields: Validating the wannier model using a microscopic calculation. *Physical Review B*, 99(3):035416, 2019.

[2] X Luo, FC Chen, JL Zhang, QL Pei, GT Lin, WJ Lu, YY Han, CY Xi, WH Song, and YP Sun. Td-mote2: A possible topological superconductor. *Applied Physics Letters*, 109(10), 2016.

[3] Di Xiao, Ming-Che Chang, and Qian Niu. Berry phase effects on electronic properties. *Reviews of modern physics*, 82(3):1959–2007, 2010.

[4] Yen-Hung Ho, Yi-Hua Wang, and Hong-Yi Chen. Magnetoelectronic and optical properties of a mos 2 monolayer. *Physical Review B*, 89(15):155316, 2014.

[5] Charles Kittel and Paul McEuen. *Introduction to solid state physics*. John Wiley & Sons, 2018.

[6] Andor Kormányos, Péter Rakyta, and Guido Burkard. Landau levels and shubnikov–de haas oscillations in monolayer transition metal dichalcogenide semiconductors. *New Journal of Physics*, 17(10):103006, 2015.

[7] Mateusz Goryca, Jing Li, Andreas V Stier, Takashi Taniguchi, Kenji Watanabe, Emmanuel Courtade, Shivangi Shree, Cedric Robert, Bernhard Urbaszek, Xavier Marie, et al. Revealing exciton masses and dielectric properties of monolayer semiconductors with high magnetic fields. *Nature communications*, 10(1):4172, 2019.

[8] Timothy C Berkelbach, Mark S Hybertsen, and David R Reichman. Theory of neutral and charged excitons in monolayer transition metal dichalcogenides. *Physical Review B—Condensed Matter and Materials Physics*, 88(4):045318, 2013.

[9] Andor Kormányos, Guido Burkard, Martin Gmitra, Jaroslav Fabian, Viktor Zólyomi, Neil D Drummond, and Vladimir Fal'ko. k· p theory for two-dimensional transition metal dichalcogenide semiconductors. *2D Materials*, 2(2):022001, 2015.

[10] Ilkka Kylänpää and Hannu-Pekka Komsa. Binding energies of exciton complexes in transition metal dichalcogenide monolayers and effect of dielectric environment. *Physical Review B*, 92(20):205418, 2015.

[11] Andreas V Stier, Nathan P Wilson, Kirill A Velizhanin, Junichiro Kono, Xiaodong Xu, and Scott A Crooker. Magnetooptics of exciton rydberg states in a monolayer semiconductor. *Physical review letters*, 120(5):057405, 2018.